IMPACT AND NATURE OF OPEN METAL SITES: A WATER AND CARBON MONOXIDE ADSORPTION STUDY ON MOF-74 ISOSTRUCTURAL MOFS

A thesis
Presented to
The Academic Faculty

by

Christine Flemming

In Partial Fulfillment
of the Requirements for the Degree
Master of Science in the
School of Chemical and Biomolecular Engineering

Georgia Institute of Technology

August 2012

IMPACT AND NATURE OF OPEN METAL SITES:
A WATER AND CARBON MONOXIDE ADSORPTION STUDY ON MOF-74 ISOSTRUCTURAL MOFS

Approved by:

Dr. Krista Walton
School of Chemical & Biomolecular Engineering
Georgia Institute of Technology

Dr. Dennis Hess
School of Chemical & Biomolecular Engineering
Georgia Institute of Technology

Dr. Yoshiaki Kawajiri
School of Chemical & Biomolecular Engineering
Georgia Institute of Technology

Date Approved

June 4, 2012

ACKNOWLEDGMENTS

I would like to thank my advisor, Dr. Krista Walton for accepting me into her research group and for her willingness to purchase all the equipment and materials that I needed to successfully complete my research goals. Under her advisement, I have learned a lot and have grown as a researcher and as a person. I would also like to thank the entire Walton group for their knowledge, constructive criticism and friendship. Without the team effort displayed by the group, I would not have been able to collect the data needed for my carbon monoxide (CO) experiments as I needed someone to check in on me periodically during my runs. I would specifically like to thank my colleague Greg Cmarik who built the pressure decay system which I used to collect my CO adsorption data. Paul Schoenecker and Yang Cai, aided me in the collection of my water adsorption isotherms for which I am very grateful. I would also like to thank Dr. Hess and Dr. Kawajiri for graciously accepting to be on my thesis committee and for their valuable input.

My sincerest gratitude goes out to all the friends I have made here at Georgia Tech who have been immensely instrumental in the successful completion of my degree. Their friendship has really kept me afloat through some very challenging times in my graduate career. The Black Graduate Student Association (BGSA) has also been a source of support for me. I would also like to whole-heatedly thank my loving family (especially my twin sister Charmaine Flemming, my mother Juliette Flemming, my aunt Yvette Burke) as well as my fiancé Jason Mills who have been extremely supportive and

encouraging, constantly checking in on me and occasionally coming to visit me here in Atlanta. Most of all I give God thanks and praise for my talents and accomplishments. Last but not least, I would like to thank my funding sources DoD PECASE Award W911NF-10-0079.

TABLE OF CONTENTS

LIST OF TABLES

LIST OF FIGURES

SUMMARY

In this work the magnesium, zinc, nickel and cobalt MOFs of the MOF-74 isostructural family are used to probe metal-dependent adsorbate interactions with water and with carbon monoxide because of their ability to generate open metal sites upon activation. An isostructural family is used so that the only variable from one MOF to another is the metal incorporated into the framework. For water adsorption isotherms with humidities up to 90%, the observed trend at 298K and 1 bar is Mg-MOF-74>Zn-MOF-74>Co-MOF-74>Ni-MOF-74. This observed trend is due to Lewis acid-base interactions. When the weight effect is removed, differences are still observed, especially below 40% relative humidity, thereby confirming that there is a metal effect. These studies revealed that PXRD alone cannot indicate the level of structural decomposition and that none of the four isostructures fully retain their structural integrity on exposure to humidified air because of microstrain and/or the presence of oxygen; more studies examining the extent of structural decomposition need to be undertaken. For carbon monoxide adsorption the general observed trend for $P < 4$ bar and temperatures of 298, 313 and 333K is Co-MOF-74>Ni-MOF-74>Zn-MOF-74>Mg-MOF-74. This trend is based on π-backbonding interactions. Here again, differences remain after removal of the weight effect, confirming the metal dependence. Notably, Co-MOF-74 has the highest CO loading at 298K and 1 bar reported so far. Both the Toth and Virial Isotherms were used to fit the CO adsorption data followed by the use of the Clausius-Clapeyron equation to find the

isosteric heats of adsorption, q^{st}. The results from the Toth isotherm are more reliable and showed that q^{st} remains constant as loading increases for Mg-MOF-74, decreases for Zn-MOF-74 and increases with loading for Co-MOF-74 and Ni-MOF-74; Ni-MOF-74 had the highest heat of adsorption at all loadings. It appears that using the Clausius-Clapeyron equation to calculate q^{st} is an inappropriate method for Ni-MOF-74 so other methods such as calorimetry are recommended. It is also recommended to model the data of all the MOFs with other isotherm models such as Sips equation and to investigate the possibility of chemisorption for the cobalt and nickel isostructures. Finally, Henry's constant results reveal that Ni-MOF-74 has the highest affinity for CO at low coverages.

CHAPTER 1

INTRODUCTION

Metal organic frameworks (MOFs) are porous crystalline materials that are made from the reaction of metal salts with organic ligands usually by solvothermal synthesis. They have many attractive properties such as extremely high surface areas as well as tunability of pore size and of chemical functionality. Consequently, there are many potential applications of metal organic frameworks including gas storage and separation, catalysis, sensors, and drug delivery.

In terms of gas separation, MOFs are of great interest in removing toxic and environmentally harmful gases from flue gas streams. However, many of these waste streams contain water vapor in addition to other undesirable components such as carbon dioxide, nitrogen oxides, sulfur oxides and carbon monoxide, so the MOFs used as selective adsorbents have to be stable under humid conditions in addition to displaying a strong affinity for the gas of interest. Water stability will allow the MOFs to be regenerated and reused provided this process is not too costly. This is therefore a motivation for the water study as well as the fact that shelf-life information for samples exposed to atmospheric air (which contains water vapor) can be obtained.

A motivation for the carbon monoxide study stems from the point alluded to in the previous paragraph about carbon monoxide being an impurity in waste gas streams. A specific example is the generation of carbon monoxide as an impurity in hydrogen

produced via steam reforming coupled with the water gas shift reaction. Additional motivation stems from the use of domestic heating systems which produce carbon monoxide at levels that could be deadly so its removal from household air is desired. In general, for gas storage applications, this affinity should be strong enough so that the gas is not prematurely released but not so strong that it can easily be delivered when needed [1].

It has been shown in prior research that MOFs that contain open metal sites (unsaturated metals centers) enhance adsorption of harmful gases. These open metal sites are generated by heating the MOF below its decomposition temperature to remove adsorbed solvent molecules such that an open coordination site results. In this work, an isostructural family of open-metal site materials referred to as M-MOF-74, M-CPO-27 or M/DOBDC (M= Mg, Zn, Ni, Co) will be studied; the MOF-74 terminology will be used in this work; the term isostructural means having the same framework topology (space group and secondary building unit).

With regard to open metal sites, the effect of metal identity on N_2 and CO_2 adsorption was studied by Caskey et al. [2] . They converted their surface areas and loadings to number of molecules per unit cell to exclude the weight effect of the different metals (Zn, Ni, Co, and Mg) in their MOF-74 family of compounds. This weight effect refers to the fact that the surface area and adsorption loading calculations are normalized by the mass of the MOF (units= m^2/g and mmol/g respectively). From their BET results, they discovered the trend that the lighter metal had the bigger BET surface area but, with the exception of Zn/DOBDC, all MOFs had 35-38 molecules of N_2 per unit cell. They argued that since each MOF had about the same number of N_2 molecules per unit cell, the

difference in surface areas was only due to the differing weights of the metals used in the synthesis and not due to any metal-adsorbate interaction.

In contrast, when CO_2 adsorption results were obtained and the number of molecules per unit cell was calculated, the values were different for each MOF in the isostructural series. This implies that each metal has a different adsorbent-adsorbate interaction with CO_2. This argument will be referred to again in Chapters 3 and 4. This paper by Caskey provided the stimulus for the work presented in this thesis to further probe this metal-dependent adsorbate interaction theory. Notably, Dietzel and co-workers asserted that the MOF-74 family of materials could be used to investigate how their properties depend on the respective metal in the framework in the same year that Caskey and co-workers published their study [3].

My objectives are as follows:

1. To study the effect of the metal on water adsorption in the MOF-74 isostructural family of MOFs. An isostructural family of MOFs was chosen so that the only variable would be the metal incorporated inside the pore structure of each MOF. Therefore, any differences in results can be directly correlated to the properties of the respective metal. To my knowledge a comparison of the water adsorption properties on this isostructural family has not been done.
2. To study the effect of the metal on carbon monoxide (CO) adsorption in the MOF-74 isostructural family of MOFs. CO adsorption is generally quite understudied in comparison to other gases such as N_2, CO_2, CH_4 and H_2.

The results will be presented as follows: Chapter 2 will detail the structure, synthesis procedures and experimental techniques including relevant theory, Chapter 3 will discuss humidity studies on the MOF-74 family and the structural integrity of the framework, Chapter 4 will discuss carbon monoxide studies including heat of adsorption data and Henry's constants, and lastly Chapter 5 will provide an overall summary and give recommendations for future work.

CHAPTER 2

MATERIALS AND EXPERIMENTAL PROCEDURES

2.1 MOF-74 Structure and Topology

The MOF-74 series of materials has a 3-dimensional honeycomb topology with one-dimensional solvent-filled channels. This as-synthesized structure has the metal atoms coordinated octahedrally (Figure 1) to six oxygen atoms, five of which are from the 2,5-dihydroxyterephthalic acid ligand and the sixth one is from water [4]. In the case of the Zn isostructure, the sixth coordination site is occupied by dimethyl formamide and not water [5]. The bound water (or DMF) molecules point toward the cavity. Due to the octahedral coordination, all of the ligand functional groups (carboxylic and alcohol) are deprotonated and all are involved in coordination towards the metal atoms [3].

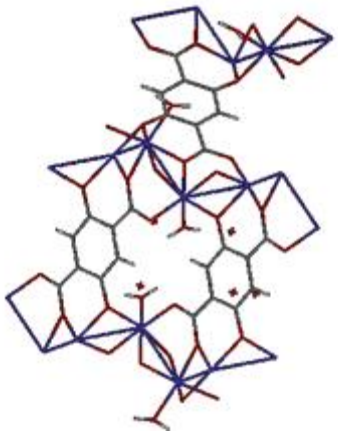

Figure 1: Octahedral Symmetry Around Metal
Blue-metal, Red-oxygen, Gray-carbon, White-hydrogen, 'x'-solvent

The average cross-sectional channel dimensions are 11.08 x 11.08$Å^2$ [4]. It should be noted that the diameter apparent to a probe molecule is naturally diminished by the probe molecule's own diameter.

There is a 60% pore volume when water is removed from the channels (Figure 2) and the coordination environment around the metal changes from octahedral to square pyramidal (Figure 3) [3, 4]. Additionally, these structures consist of 1D 3-dimensional helical chains but the structure consists of a racemic mixture of chains of both handedness so stereoselective adsorption is not possible (Figure 4) [3].

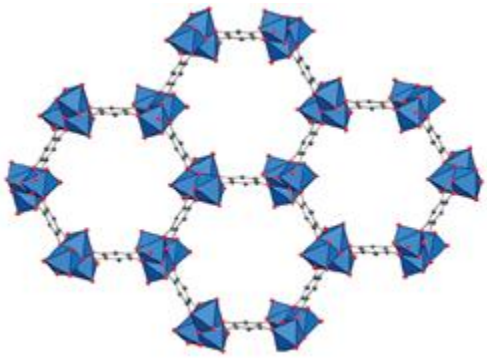

Figure 2: Packing Along [001] Direction. Figure taken from [3]

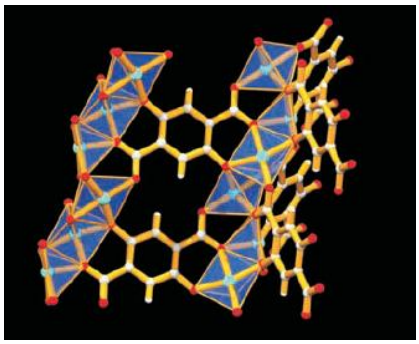

Figure 3: Square Pyramidal Environment on Solvent Removal. Figure taken from [4]

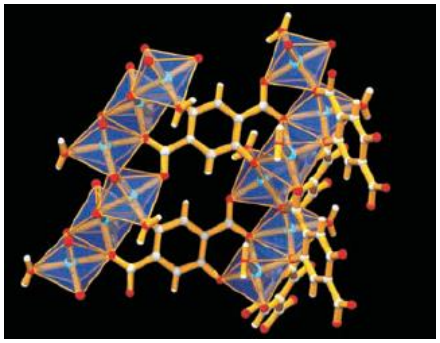

Figure 4: View of Opposite Handedness of Neighboring Helical Chains. Figure taken from [4]

2.2 Synthesis Methods

Previously reported synthesis procedures were followed for each MOF with a few minor changes in the case of magnesium and zinc[6]. These reported synthesis procedures followed, varied slightly from the original synthesis papers [3-5, 7]. The samples obtained after synthesis and solvent exchange were the as-synthesized samples. These as-

synthesized samples were stored in filter paper and submersed in methanol until they were ready to be used.

2.2.1 Magnesium (Mg)-MOF-74

0.112 g of 2,5-dihydroxyterephthalic acid (DOBDC) and 0.475 g of $Mg(NO_3)_2.6H_2O$ were dissolved in 51 ml of liquid that comprised of dimethylformamide (DMF), ethanol and water in a 15:1:1 ratio and sonicated until a homogeneous solution resulted. This solution was poured into five 20 ml glass vials and placed into an isothermal oven for 21 hours at 125°C. At the end of the synthesis, the vials were allowed to cool before filtering off the supernatant liquid. The Mg-MOF-74 was then solvent-exchanged in methanol for three days using a Soxhlet extractor.

2.2.2 Zinc (Zn)-MOF-74

1.00g of DOBDC and 4.95 g of $Zn(NO_3)_2.6H_2O$ were dissolved in 100 ml of DMF in a glass jar and sonicated until a homogeneous solution resulted; during sonication, 5 ml of water was added. The glass jar was then placed in an isothermal oven for 21.5 hours at 110°C. At the end of the synthesis, the jar was allowed to cool before filtering off the supernatant liquid. The Zn-MOF-74 was then solvent-exchanged in methanol for four days using a Soxhlet extractor.

2.2.3 Cobalt (Co)-MOF-74

0.5g of DOBDC and 1.5 g of $Co(NO_3)_2.6H_2O$ were added to a glass jar, dissolved in 210 ml of liquid that comprised of DMF, ethanol, and water in a 1:1:1 ratio and sonicated until a homogeneous solution resulted. The glass jar was then placed in an isothermal oven for 2 days and 18 hours at 100°C. At the end of the synthesis, the jar was allowed to cool before filtering off the supernatant liquid. The Co-MOF-74 was then solvent-exchanged in methanol for four days using a Soxhlet extractor.

2.2.4 Nickel (Ni)-MOF-74

0.5g of DOBDC and 1.5 g of $Co(NO_3)_2.6H_2O$ were added to a glass jar, dissolved in 210 ml of liquid that comprised of DMF, ethanol, and water in a 1:1:1 ratio and sonicated until a homogeneous solution resulted. The glass jar was then placed in an isothermal oven for 2 days and 18 hours at 100°C. At the end of the synthesis, the jar was allowed to cool before filtering off the supernatant liquid. The Co-MOF-74 was then solvent-exchanged in methanol for four days using a Soxhlet extractor.

2.3 Characterization

Nitrogen adsorption and Powder X-Ray Diffraction (PXRD) experiments were performed on the as-synthesized samples that were used for water and carbon monoxide adsorption experiments as well as on the regenerated samples post water adsorption. Nitrogen adsorption isotherms were collected at 77K using a Quantachrome Quadrasorb system and BET surface areas were calculated automatically by the software (Equations 1 to 3). Powder XRD diffractograms were collecting using a PANalytical x-ray diffractometer.

2.3.1 BET (Brunauer-Emmett-Teller) Equation

All nitrogen sorption data were processed using the BET equation. The assumptions in the BET model are as follows: (1) infinite multilayer adsorption (2) no adsorbate-adsorbate (lateral) interactions (3) the rate of adsorption of any layer equals the rate of desorption from the layer above it (4) the heat of adsorption of the second and all subsequent layers equals the heat of liquefaction of the adsorbate.

$$\frac{P}{V(P_o - P)} = \left[\left(\frac{C-1}{V_m C}\right)\right]\frac{P}{P_o} + \frac{1}{V_m C} \qquad (1)$$

$$\underbrace{\frac{P/P_o}{V(1 - P/P_o)}}_{y} = \left[\left(\frac{C-1}{V_m C}\right)\right]\underbrace{\frac{P}{P_o}}_{x} + \frac{1}{V_m C} \qquad (2)$$

P: equilibrium pressure

P_0: saturation pressure

V: volume of gas adsorbed

V_m: volume of gas adsorbed in a monolayer

C: BET constant

V_m is needed to calculate the surface area and it is obtained from Equation 2 by first solving for C by dividing the slope $[(c-1)/V_mC]$ by the y-intercept $1/V_mC$ and then substituting back into either the slope or y-intercept equation. The surface area, SA equation is calculated as follows:

$$SA = \frac{V_m N_A}{V}\alpha \qquad (3)$$

SA: surface area per mass of solid (m^2/g)

V_m: volume of gas adsorbed at STP per mass of solid

N_A: Avogadro's number of molecules (6.022×10^{23} molecules/mole)

V: volume per mole of gas at STP

α: area of adsorbed nitrogen molecule (16.2 $Å^2$)

2.4 Adsorption Isotherm Measurement

2.4.1 IGA-003 Microbalance

Water adsorption isotherms were collected via a method used in previous work on an IGA-003 microbalance from Hiden Isochema [8]. The isotherms were collected at 298K and at 1 bar over a range of humidities from 0 to 90%. Higher humidity ranges were not possible due to condensation issues. All the MOFs were loaded wet (having been kept under methanol) and activated in situ at 200°C to remove residual methanol and any water that may have been adsorbed during sample loading. The carrier gas was dry air, some of which was bubbled through a vessel of deionized water in order to humidify the stream. Using two mass flow controllers to vary the ratio of saturated air to dry air, the humidity level was varied. The total gas flow rate was 200 cm^3/min throughout the experiment and 24 hours was the maximum time allotted for each point to reach equilibrium. After collecting the isotherm, each sample was regenerated.

2.4.2 Pressure Decay

All carbon monoxide (CO) isotherms were collected on a pressure decay system (Figure 5) that was built by a fellow group member, Greg Cmarik. Valves 1 and 2 were

associated with the right sample cell and valves 3 and 4 were associated with the left sample cell (Figure shows only 1 sample cell). With this setup, two samples could therefore be run simultaneously and a maximum pressure of 6 bar could be reached. Adsorption isotherms were collected at 298, 313, and 333K (20, 40 and 60°C) so that the heat of adsorption could be calculated for each MOF, as will be described in detail in Chapter 4. Prior to the first CO run, the samples were activated (heated under vacuum) between 150 and 200°C overnight to remove all solvent molecules and to generate open metal sites. Activation was done outside of the water bath with heating tape as the maximum operating temperature of the water bath was only 70°C. As the samples were loaded wet (having been submersed in methanol), the weight of the activated sample was recorded at the end of the experiment when the sample was removed from the sample holder. The weight of the wet sample was still recorded to get an idea of the weight loss experienced by the sample on activation.

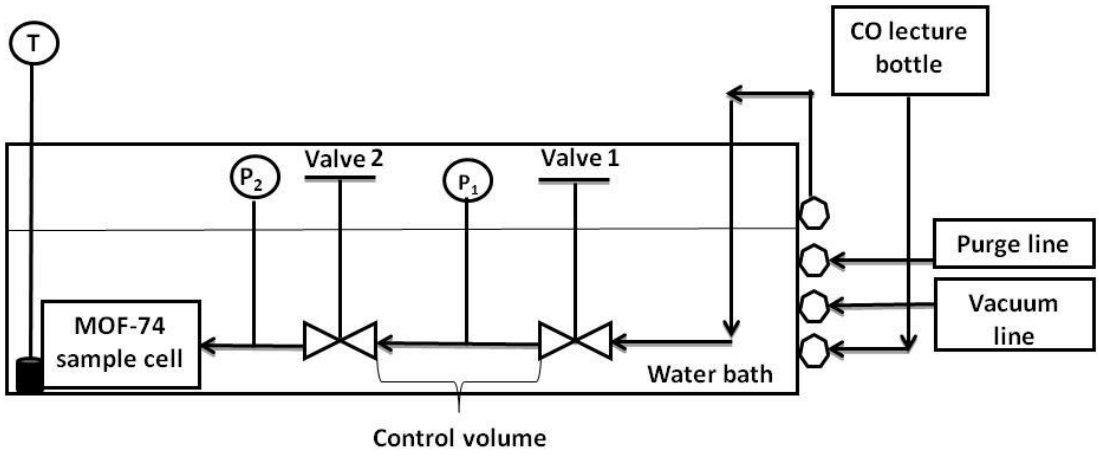

Figure 5: Schematic of Pressure Decay System

The entire experiment (pressure decay and CO lecture bottle) was contained in the fume-hood and all necessary safety precautions were taken while running the experiment. These included having a CO personal detector as well as a CO detector beside the CO cylinder, and having an assigned person check in periodically to make sure that no major issues arose.

During the experiment itself, CO gas was allowed into the first section of each cell. This was done by opening valves 1 and 3 while having valves 2 and 4 closed; the pressures were recorded. In this way, the number of moles of gas allowed into each cell could be calculated since the temperature was set, the pressure was recorded and the control volume was known. Valves 1 and 3 were then closed and valves 2 and 4 were quickly opened and closed. After equilibrium was reached for that point (approximately an hour), the pressures were recorded so that the number of moles adsorbed could be calculated using the Peng Robinson equation as will be discussed in Chapter 4. This was again possible because the temperature was known, the pressure was recorded and the sample volume was known. The difference between the number of moles in valves 1 and 2 and between valves 3 and 4 gave the number of moles of CO adsorbed. More CO was incrementally allowed into the system by this procedure until the number of data points desired was collected. Special attention was paid to the low pressure region (corresponding to low loadings) since metal-adsorbate interactions are dominant here.

CHAPTER 3

HUMIDITY ADSORPTION STUDIES ON MOF-74 ISOSTRUCTURAL COMPOUNDS

3.1 Background

Instead of investigating water adsorption alone, many papers have actually investigated the effect of humidity on CO_2 (combined stream of water vapor and CO_2) adsorption in the context of CO_2 capture from flue gas. Specifically, Kizzie and co-workers have examined breakthrough curves for Zn, Ni, Co and Mg/DOBDC (same materials used in this work) under dry and humidified surrogate flue gas conditions and have found, in agreement with Caskey and coworkers, that Mg/DOBDC has an enormous capacity for CO_2 under dry conditions; the best CO_2 capacity recorded to date [2, 9].

However, after exposure to 9% relative humidity and subsequent thermal regeneration, its CO_2 capacity diminishes significantly to about 33% of its original value. This makes it impractical for cyclical industrial CO_2 capture since power plant flue gas streams contain about 15% and 6% H_2O for gas-fired and coal-fired flue gas respectively [10]. However, it is quite possible that the regeneration temperature of 150°C is not high enough to remove all of the strongly adsorbed water molecules. This premise is supported by Schoenecker and co-workers who heated Mg-MOF-74 to a temperature as high as 300°C in an effort to obtain the highest accessible surface area without decomposing the sample.

However, the surface area obtained was still far below the value obtained prior to water exposure. Hence, they suggested that some structural decomposition has occurred and is responsible for the reduced capacity [8]. Consequently, this decomposition is most likely the cause for the reduced surface area obtained; this will be discussed in more detail later.

Also in the work by Kizzie and coworkers, Co/DOBDC actually retained the highest percentage of its original CO_2 capacity (85%) after exposure to 70% relative humidity and subsequent regeneration with Ni/DOBDC retaining the second highest percentage at 61%. Interestingly, in a paper by Liu et al, Ni/DOBDC retained 92% of its original CO_2 capacity after exposure to steam at 100°C but the steam contained no more than 10% water vapor. Liu and coworkers attribute this good CO_2 capacity retention to the slow regeneration procedure they employed which avoided the sudden vaporization of adsorbed water. Meanwhile, Mg/DOBDC only retained 49% of its CO_2 capacity under similar conditions despite better PXRD with its unsteamed counterpart than Ni/DOBDC had with its unsteamed equivalent [11].

Liu et al. also make the point that CO_2 capacities are related to the density of unsaturated metal centers (or open metal sites) and that the metal ion with the more negative standard reduction potential is more prone to react with water or oxygen in air and be subsequently oxidized. This would decrease the number of open metal sites and therefore decrease its capacity. On the contrary, Dietzel and co-workers opposed the standard reduction potential theory in an earlier paper by saying that magnesium is not susceptible to redox

reactions under the conditions present and proposed instead that the framework collapse is related to oxygen in the air reacting with the organic ligand [3].

Low and co-workers investigated the hydrothermal stability of a number of MOFs via the use of a high throughput steam apparatus in combination with a quantum mechanical cluster model[12]. They found that predicted activation energies for ligand displacement with water correlate with experimentally observed hydrothermal stabilities. Convinced that their cluster model could accurately rank the relative stability of a given group of MOFs, they performed a virtual high throughput screening (VHTS) on seven different MOFs, and the results exhibited a fairly good match to experimental data. Zn-MOF-74 was one of the tested MOFs and it was found to be hydrothermally stable in up to 50% steam and 325^0C. The strong structural stability of Zn-MOF-74 was attributed to (i) edge-sharing between metals in addition to coordination of two types of functional groups on each linker (ii) a six-coordinate environment on solvation making displacement from an incoming water ligand less likely and (iii) open metal sites generated on activation which when water coordinates reduces the probability of an insertion into a metal-ligand bond and consequent ligand displacement.

3.2 Results and Discussion

All experimental methods including MOF synthesis procedures were described in Chapter 2.

3.2.1 Water Adsorption Isotherms

Water adsorption isotherms for the four MOF-74 isostructures are shown in Figure 6.

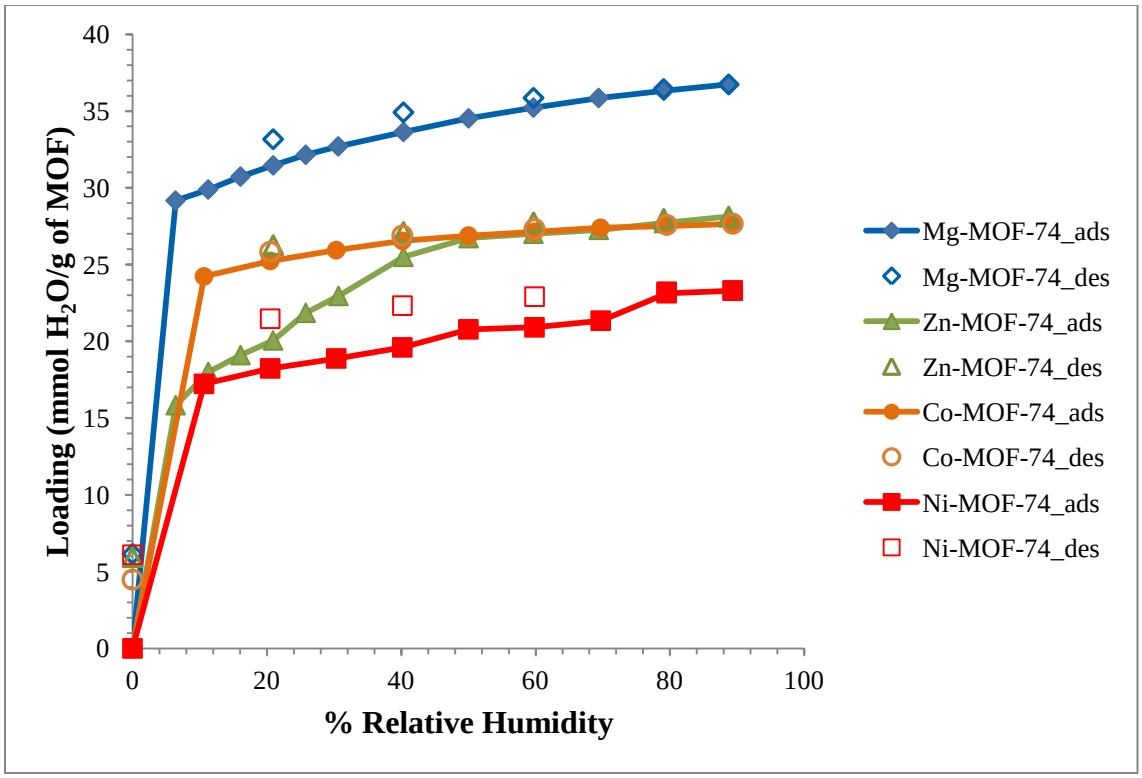

Figure 6: Water Adsorption Isotherms for MOF-74 Isostructural Series at 298K and 1bar. Ads: adsorption; Des: desorption. Lines are to help guide the eye.

As expected for open metal site MOFs, all four MOF-74 materials show a very high affinity for water (Type I isotherm), especially MOF-74-Mg which adsorbs almost 30 mmol of H_2O/g of adsorbent at a relative humidity of only 11%. This is a higher adsorption capacity than that achieved by any of the other MOFs at the maximum tested humidity of almost 90%. Also, Mg-MOF-74 subsequently adsorbs about 20% more water. Zn-MOF-74 has the next highest loading with Co-MOF-74 almost matching it exactly at the higher humidities and finally Ni-MOF-74 has the lowest water loading. As mentioned in the paper by Schoenecker and co-workers, these Type 1 water isotherm shapes are similar to those obtained for zeolites 5A and 13X which also contain open metal sites [13].

Mg-MOF-74 was correctly predicted to have the highest loadings based on the fact that water is a hard Lewis base due to its relatively small size and relatively high electronegativity and Mg^{2+} is a hard Lewis acid due to its high charge to size ratio (charge density) and its low electronegativity. Hard Soft Acid Base (HSAB) theory asserts that hard Lewis bases prefer to bind to hard Lewis acids. Notably, it was already known qualitatively that Mg-MOF-74 adsorbs more water than Ni-MOF-74 based on the fact that a higher temperature is needed to remove water molecules [3]. Zn^{2+}, Co^{2+}, and Ni^{2+} metals are all considered borderline Lewis acids. Consequently, their adsorption behavior should be somewhat comparable and any differences are expected to arise from differences in atom sizes or in electronegativities since they all have the same charge. Atom size, charge and electronegativity are characteristics used to assess the hardness of a Lewis acid. Evidently, the size differences are negligible. Andreini and co-workers

report the ionic radii of Zn^{2+} and Co^{2+} to be 0.74 Å and 0.75 Å respectively [14]. Ni^{2+} was not reported but should be between 0.74 and 0.75 Å based on its position in the periodic table. Therefore any differences observed are due to differences in electronegativities (Co= 1.88 and Ni= 1.91) which are more substantial than the size differences and all other things being equal, a smaller electronegativity makes for a harder acid because it means a higher tendency toward the formation of a cation. When the weight effect was removed differences persisted as will be discussed further in section 3.2.3.

HSAB theory is a qualitative theory. However, some quantitative ways of determining Lewis acidity have been proposed. One example is the equation proposed by Zhang which gave a Lewis acidity, Z, that is dependent on both the electrostatic force and the covalent bond strength (Equation 4) [15].

$$Z = {}^{z}/_{r_k{}^2} - 7.7\chi_z + 8.0 \qquad (4)$$

${}^{z}/_{r_k{}^2}$: electrostatic force

z: charge number of the atomic core (# of valence electrons)

r_k: ionic radius

χ_z: electronegativity (covalent force). These values were taken from Zhang's previous work [16]

From Zhang's Lewis acidity values, the trend of highest to lowest acidity is Mg>Zn>Co>Ni which follows the observed trends. See Table 1 for a comparison of ionic radii, atomic electronegativity and Lewis acid strength of open metal sites.

Table 1. Comparison of Lewis Acidity-Related Properties and Lewis Acidities for MOF-74 Open Metal Sites

	Ionic Radius/Å	Atomic Electronegativity (Pauling scale)	Lewis Acid Strength
Mg^{2+}	0.72	1.31	1.402
Zn^{2+}	0.74	1.65	0.656
Co^{2+}	0.75	1.88	0.356
Ni^{2+}	0.74-0.75	1.91	0.293

When comparing the adsorption and desorption water isotherms, Type H2 hysteresis is observed for each MOF especially for the Ni-MOF-74 and Zn-MOF-74. This hysteresis indicates the difficulty in removing adsorbed water from the MOF [8]. In fact, after desorption each MOF retains about 5 mmol of water/g of MOF and this shows that the water cannot be fully desorbed under dry air conditions.

3.2.2 Investigation of Structural Stability

To investigate the structural effect of water loading on the MOFs, Powder X-ray diffractograms (Figures 7 to 10) and BET surface areas (from nitrogen sorption isotherms) (Table 2) were collected at the end of each H_2O adsorption experiment after sample reactivation to remove any remaining adsorbed water. For all the isostructures

except nickel, the PXRD's suggest their robustness against water exposure. However, all four isostructures have significantly reduced BET surface areas.

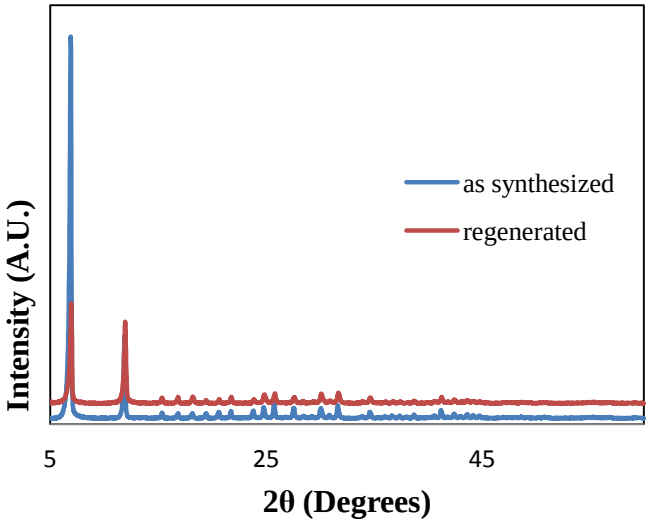

Figure 7: PXRD of Mg-MOF-74 Made Before and After Water Exposure

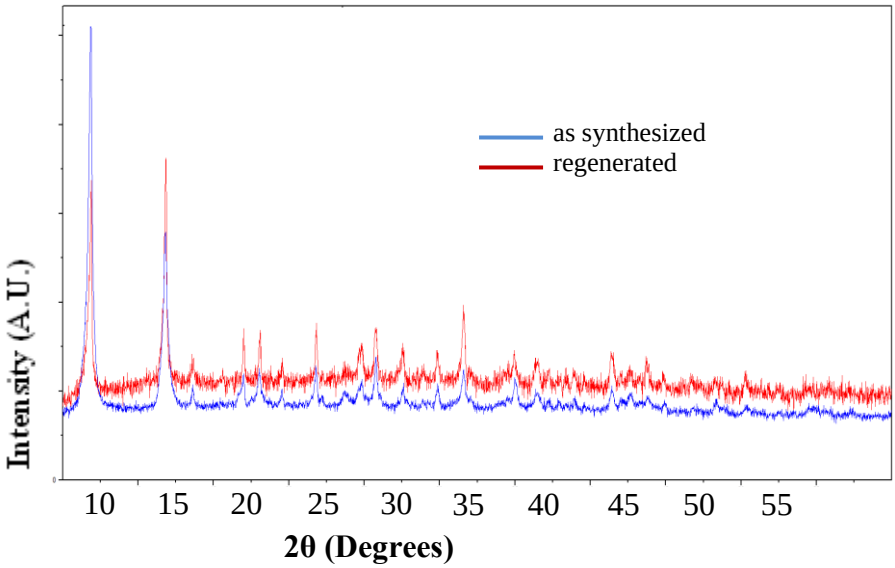

Figure 8: PXRD of Zn-MOF-74 Made Before and After Water Exposure

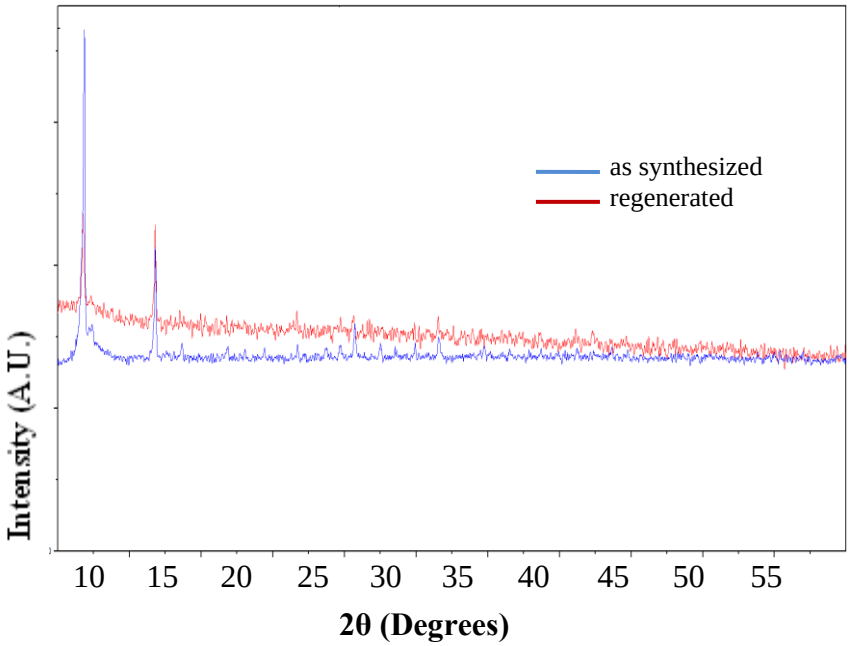

Figure 9: PXRD of Co-MOF--74 Made Before and After Water Exposure

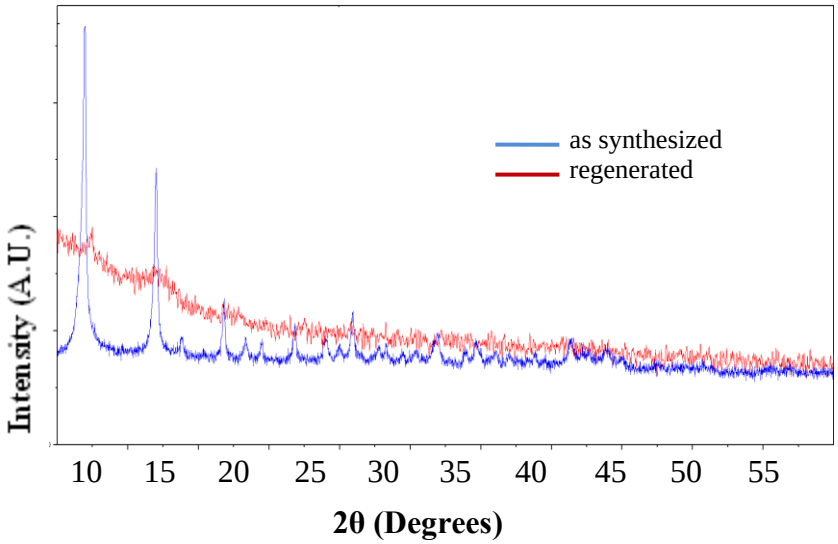

Figure 10: PXRD of Ni-MOF-74 Made Before and After Water Exposure

Table 2. Nitrogen Sorption Data for As-Synthesized and Regenerated Samples

Material	Measured surface area (m^2/g)				As-synthesized Activation Conditions	Regeneration Conditions
	Before	After	% Surface Area Loss	Previously Reported		
Mg-MOF-74	1400	238	83	1206[a]; 1495[c]	250°C overnight	250°C for ~12 hrs (initial) and then at 300°C for ~12 hrs [8]
Zn-MOF-74	842	104	88	496[a]; 632[b,] 816[d]	150°C overnight in vacuum oven and then at 200°C for a few hours	100°C overnight and at 200°C for a few hours
Co-MOF-74	984	112	89	835[a]; 1080[c]	150°C overnight	200°C for about 4 hrs
Ni-MOF-74	753	53	93	599[a]; 1070[e]	150°C overnight	200°C for about 4 hrs

a- ref[6]; b-ref[17]; c-ref[2]; d-ref[18]; e-ref[7]

As mentioned in section 3.2.1, not all of the adsorbed water has been desorbed under the dry air conditions. More water is removed upon regeneration but even if some water remains, it cannot account for such a drastic reduction in surface area. The more likely cause is that there is partial structural decomposition of all of the isostructures which is evident in the PXRD for Ni-MOF-74 only. This is at first counter-intuitive but evidently, if any part of the sample is crystalline, Bragg peaks will be observed even if other parts of the sample have decomposed. Hence partial structural decomposition is quite probable and PXRD alone is not sufficient to gage the structural integrity of a given MOF material.

This point was made by both Kizzie and co-workers and Schoenecker and coworkers [8, 9]. If the x-ray diffractogram shows significant structural loss one can expect to obtain low surface areas but when small or no mismatches in XRD data occur, one cannot predict the amount of surface area loss that has occurred [8]. This latter point is supported in this work since all the MOFs except the Ni version have good XRD patterns yet drastically decreased surface areas. As for Ni-MOF-74, the x-ray data shows significant framework collapse (Figure 10) which is also verified by the obtained BET surface areas (Table 2). As previously mentioned, despite Ni-MOF-74's poor XRD data obtained after exposure to10% steam at 100°C, Liu et al. found that it retained 92% of its original CO_2 capacity and Mg-MOF-74 only retained 49% of its capacity under similar conditions despite its good XRD results[11]. This is evidence that not only is PXRD on its own inadequate to predict structural integrity, it is also inadequate in predicting capacity; a key point which was also expressed by Kizzie and coworkers [9].

In terms of partial decomposition, Dietzel and co-workers showed, via variable-temperature powder XRD, that loss of structural integrity of Mg-MOF-74 starts at 160°C in air- before the complete decomposition temperature indicated by the TGA. As a result, they warn against judging thermal stability solely on the basis of TGA curves- an issue which arises if activating under nitrogen and in air but not if under dynamic vacuum. They suggested that this decomposition is related to the oxygen in the air reacting with the organic ligand. Even though the water adsorption experiments in this study were only carried out at 25°C, the fact that the thermal stability of the Mg-MOF-74 is lower under air atmosphere as compared to an inert or vacuum atmosphere should be noted [3].

Thermal stability data is listed in Table 3. All activations and regenerations of each material were done under dynamic vacuum and all temperatures were chosen to be below the decomposition temperature as obtained from thermal gravimetric analysis (TGA) and from thermodiffractometry in the case of Co-MOF-74 and some of the Mg-MOF-74 data. These stabilities represent the maximum temperature these MOFs can be heated to before complete structural decomposition of the framework occurs.

Table 3. Thermal Stabilities of MOF-74 Isostructural MOFs

Material	Thermal Stability/°C
Mg-MOF-74	400 in N_2, 305 in air, 430 in dynamic vacuum [3]
Zn-MOF-74	400 [5]
Co-MOF-74	320 under inert atm; 234 in air [4]
Ni-MOF-74	350 in N_2, between 240 & 250 in air [7]

Besides the presence of oxygen, microstrain of the MOF-74 frameworks on repeated dehydration is likely to have caused partial structural collapse. Microstrain occurs in these materials due to the expansion and contraction of the framework in order to compensate for the removal of water molecules from the pore space. Dietzel and coworkers carried out detailed variable temperature PXRD experiments on Co- and Zn-MOF-74 during the dehydration process (the removal of water molecules from the as-synthesized samples). The experiments were done on a beamline BM01A at ESRF. They found that no significant microstrain is introduced upon dehydration for Co-MOF-74 but there is some introduced for the zinc isostructure. In fact, on heating up to 500°C, five

different phases (five different PXRD patterns) were observed. Even though no significant microstrain was observed for Co-MOF-74 during this initial dehydration, it is possible that some strain is introduced on repeated dehydration that occurs during reactivation of the sample after water exposure.

These authors also noted that the variable temperature X-ray powder patterns of Ni-MOF-74 look very similar to those of Co-MOF-74 and they therefore expect its dehydration process to be the same but analogous detailed studies were not performed to confirm this [19]. In addition, Dietzel and coworkers report that Ni-MOF-74 breathes on dehydration [20]. This breathing phenomenon could lead to structure microstrain. As for Mg-MOF-74, Dietzel and co-workers believe that its framework remains essentially unperturbed by dehydration because their variable temperature x-ray diffractograms show fairly consistent reflection positions [3]. However, as with Co-MOF-74, microstrain may be introduced on repeated dehydration.

3.2.3 Number of Molecules per Unit Cell

Following what Caskey and co-workers did for their N_2 sorption and CO_2 data (See Introduction) [2], the number of molecules per unit cell was calculated for both the N_2 sorption data and the H_2O adsorption data. This was done to normalize the data for the weight effect of the different metals since both sets of results are given in per mass units. If the number of molecules per unit cell is different from one MOF to another, there is a metal effect. The results for the N_2 sorption data are tabulated (Table 5) and the results for the H_2O data are shown graphically (Figure 11). As a preliminary step, the number of

molecules per unit cell for Caskey's N_2 sorption data was recalculated to ensure that the calculation method was consistent (Table 4).

Table 4. Comparison of Number of N_2 Molecules per Unit Cell Results for MOF-74 Materials Used by Caskey and Co-Workers [2]

Material	BET Surface Area (m^2/g) [2]	Number of N_2 Molecules per Unit Cell [2]	Number of N_2 Molecules per Unit Cell
Mg-MOF-74	1495[c]	35-38	33.5
Zn-MOF-74	816[d]	26	24.5
Co-MOF-74	1080[c]	35-38	31.1
Ni-MOF-74	1070[e]	35-38	30.7

c-ref[2]; d-ref[18]; e-ref[7]

The values calculated were a bit lower than the values calculated by Caskey and co-workers but this is probably due to round-off errors. Like Caskey, the number of N_2 molecules per unit cell for zinc was noticeably lower than the others and this they attributed to incomplete activation, pore blockage, or partial collapse of structure on activation [2].

The calculation for the number of molecules per unit cell for the MOF-74 materials used in this paper are shown for both the nitrogen sorption and the water adsorption isotherm data (Table 5 and Figure 11 and Appendix G for sample calculations). From the results one can conclude that, excluding the weight effect, there are still differences between each of the MOFs- even for the nitrogen sorption data. This conclusion differs from

Caskey and co-workers who considered there to be no difference between the nitrogen sorption of each MOF when the weight effect was removed even though the molecules per unit cell differed (Table 4). Interestingly, they did a similar calculation for their CO_2 isotherm results and concluded that without the weight effect the MOFs differed from each other since the number of molecules per unit cell was about 12, 7,7 and 4 for Mg, Co, Ni, and Zn respectively-differences comparable to the differences in their N_2 sorption results.

It could be argued that in fact nitrogen, even though often considered to be inert, has varying interaction with each metal because of its quadrupole. Convincing evidence of a significant interaction between dinitrogen and Ni-MOF-74 has been provided by Chavan and co-workers [21]. This interaction has been observed from a temperature as high as 295K and at low pressure. This is significant because N_2 adsorption is usually observed only at very low temperatures and high pressures. Additionally, in the book by Rouquerol, Rouquerol and Sing, N_2 displayed dissimilar physisorption behavior to argon on hydroxylated silica, rutile, and zinc oxide despite their similar physical properties. This is because nitrogen's field gradient dipole (quadrupole) is significant when nitrogen is adsorbed on polar or ionic surfaces [22]. The open metal sites inside the MOFs are ionic.

Table 5. Number of N_2 Molecules per Unit Cell for MOF-74 Materials Used in H_2O Experiments

Material	BET Surface Area (m^2/g)	Number of N_2 Molecules per Unit Cell
Mg-MOF-74	1400	31.3
Zn-MOF-74	842	25.2
Co-MOF-74	984	28.3
Ni-MOF-74	753	21.6

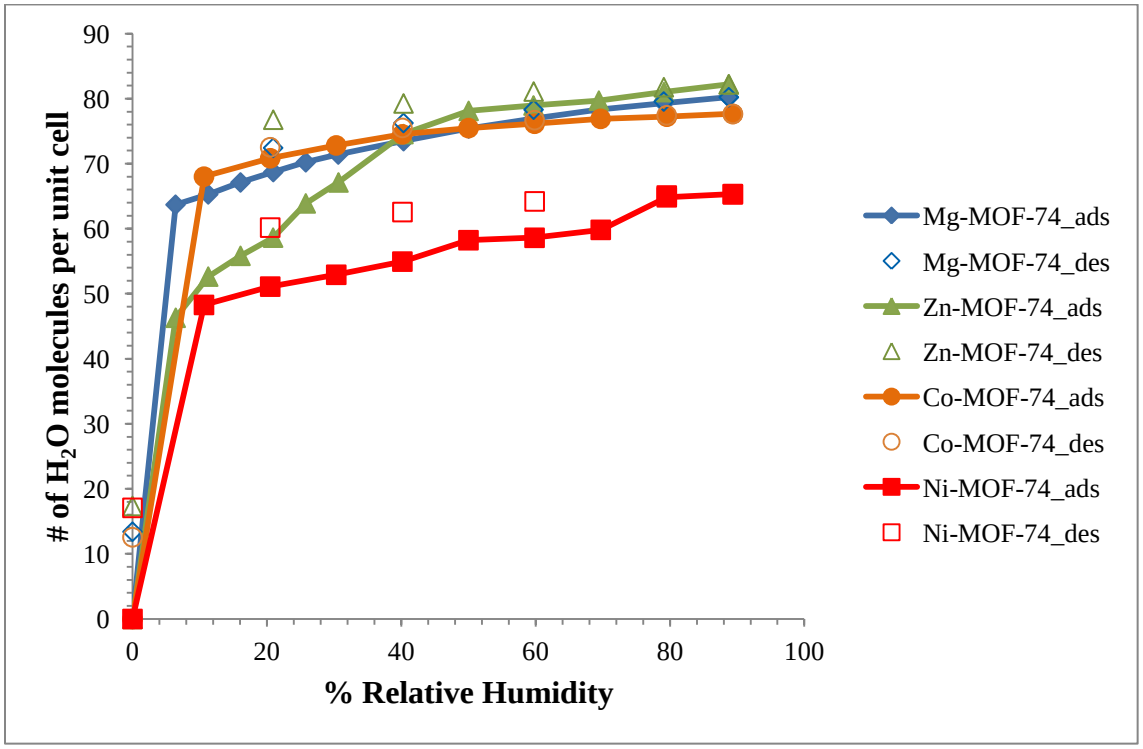

Figure 11: Number of H_2O Molecules per Unit Cell
Ads: adsorption; Des: desorption. Lines are to help guide the eye.

It is interesting that when the weight effect is removed from the H_2O isotherm data, the loadings for Mg-, Zn- and Co- loadings coincide at relative humidities ≥ 40% while the Ni-MOF-74 isotherm remains significantly lower. At these higher humidities, most if not all of the open metal sites have been occupied by water molecules so adsorbent-adsorbate interactions (determined by HSAB theory) are no longer dominant. It becomes more a matter of how much space is left on the pore surface and in the pore volume. Thus, the overlapping isotherms observed suggest that surface area and subsequently pore volume is what determines the loading. However, one should note that these MOFs, especially the nickel isostructure could be decomposing during exposure to the oxygen-containing humidified air stream and this would affect loadings. Notably, differences persist at humidities below 40%.

3.3 Conclusions

As expected from HSAB theory, the loading trend from highest to lowest loading at 298K and I bar is as follows: Mg-MOF-74> Zn-MOF-74>Co-MOF-74>Ni-MOF-74. The lower humidity region is the region of interest because this is where adsorbent-adsorbate interactions are dominant. All of the isotherms are of Type 1 indicating the affinity of all the MOFs for water and they all display H2 hysteresis especially the zinc and nickel isostructures.

PXRD alone is not sufficient to deduce structural integrity but from these results, it is observed that Ni-MOF-74 has clearly undergone significant decomposition. No loss of structural integrity is observed from the PXRD of the other MOFs yet all four isostructures suffer severe loss of surface area that cannot be explained solely by

undesorbed water molecules alone. Partial structural decomposition is thus believed to have occurred for all of the MOFs due to microstrain introduced on repeated dehydration and perhaps also the presence of oxygen in the humidified air stream; however, the extent of decomposition is unknown and needs to be investigated further.

Finally, without the weight effect, there are still differences between each isostructure since the number of molecules per unit cell is different from one MOF to another. For the nitrogen sorption experiments this difference occurs because of N_2's quadrupole and for the water isotherms below 40% relative humidity, it occurs because of differences in Lewis acidity. Above 40% relative humidity these differences are obscured for all MOFs except the nickel isostructure but this may be due to more structural decomposition occurring for this MOF in comparison to the other MOFs.

CHAPTER 4

CARBON MONOXIDE ADSORPTION STUDIES ON MOF-74 ISOSTRUCTURAL COMPOUNDS

4.1 Background

Carbon monoxide (CO) is a very weak Brønsted-Lowry base and a weak Lewis base. It is produced by incomplete combustion (lack of sufficient oxygen) of fuel in internal combustion engines, coal, charcoal, and natural gas among others. In industry, CO is the main impurity of hydrogen produced via steam reforming of natural gas coupled with the water gas shift reaction (Reactions a and b) and it is present in the off-gases from steel plants and other metallurgical plants. It also poisons the metallic catalyst deposited on electrodes used in hydrogen fuel cells [23, 24].

Steam reforming reaction: $CH_4 + H_2O \rightarrow CO + 3\ H_2$ (a)

Water-gas shift reaction: $CO + H_2O \rightarrow CO_2 + H_2$ (b)

In addition, carbon monoxide is naturally produced in the body and may be a neurotransmitter, but when inhaled, it can be deadly because of its interaction with hemoglobin in the blood. There are four iron ions in each hemoglobin molecule and, under normal operation each molecule therefore reacts with four molecules of dioxygen at the surface of the lungs to form oxyhemoglobin. This bonding is weak in order to

enable transport and subsequent release of dioxygen to muscles and other energy-utilizing tissues. However, when CO is inhaled, it preferentially binds to Fe^{2+} in hemoglobin in the blood to form carboxyhemoglobin. In fact carbon monoxide has a 300 fold greater affinity for blood than dioxygen [25]. Symptoms of carbon monoxide poisoning are headache, nausea, vomiting, dizziness, fatigue, seizure, coma which can lead to fatality.

Despite its potential harm, carbon monoxide is a universal probe molecule. Vibrational spectroscopy with the use of adsorbed probe molecules such as CO is one of the most common methods for studying the composition and structure of the surface functional groups of supported metal catalysts. The vibrational spectrum is so useful because it reflects properties of the structure as a whole as well as properties of individual bonds [26]. CO such a useful probe molecule particularly for acid sites because it is a weak base. Its weak basicity enables it to probe varying concentrations and strengths of acid sites whereas strong bases would only be able to detect strong acid sites. The stretching frequency varies with Lewis acidity: the higher the stretching frequency, the stronger the Lewis acid site. In addition, CO can bind to sites in either a terminal or a bridged fashion. When it binds terminally, the stretching frequency is higher [26].

There has been limited work done on CO adsorption in MOFs in literature especially in comparison to gases such as N_2, CO_2, CH_4 and H_2. Some work has been done by Chavan and co-workers on the interaction of CO with Ni-MOF-74 using a combination of techniques: infrared (IR), Extended X-ray Absorption Fine Structure (EXAFS), X-ray Absorption Near Edge Spectroscopy (XANES), UV-vis spectroscopy, and calorimetry.

From their work they found that Ni-MOF-74 strongly coordinates to CO at room temperature forming 1:1 linear Ni^{2+}---CO adducts and that π-backdonation (π-backbonding) must be considered. The strength of the Ni^{2+}---CO interaction was ranked as follows: oxides < MOFs <zeolites. These authors even collected CO adsorption isotherms in the very low pressure region (<0.1 bar) and Type 1b behavior was observed. In addition, the differential adsorption heat was almost constant with loading thus providing evidence for the 1:1 adducts. From XANES, they observed that water removal causes a symmetry change from octahedral-like to square-pyramidal like (as observed by Dietzel et al. for Co-MOF-74 [4]) and that CO adsorption almost completely restores the octahedral symmetry present in the as-synthesized material [23].

In another paper by Chavan and co-workers, Ni-MOF-74 was investigated for nitrogen (N_2) adsorption with which it forms linear adducts like it does with CO. It does so almost at room temperature (295K) which is unusual, as mentioned in chapter 3.2.3, since reported nitrogen complexes are at low temperature and high pressure [21]. Also like CO, N_2 restores the octahedral symmetry present before solvent removal. Ethylene (C_2H_6) adsorption was also investigated via IR and it was found that C_2H_6 is only weakly perturbed by the Ni^{2+} site [21].

Computational experiments were also carried out by Valenzano and co-workers on Mg-MOF-74 for the adsorption of CO, N_2 and CO_2. Similar to the nickel isostructure, Mg-MOF-74 forms a linear complex with both CO and N_2. However with CO_2 it forms an angular complex. Dispersion interactions were found to be significant for the adsorption

of all three gases [27]. Since Ni-MOF-74 and Mg-MOF-74 have been shown to form linear adducts with CO in which the CO molecules are bound via the carbon, it is assumed that the same is true for Zn- and Co-MOF-74. In other work, Saha and Deng measured CO adsorption on zeolite 5A, zeolite 13X, MOF-5 and MOF-177 and found that at 298K and 1 bar, zeolite 5A had the highest adsorption loadings but at higher temperatures MOF-177 surpassed the others [28].

Work has also been done on gas mixtures containing CO. In particular, simulation studies were performed by Karra and Walton on the separation of CO from binary mixtures involving CH_4, N_2, and H_2 with the famous CuBTC (HKUST-1) MOF. They found that CuBTC selectively adsorbed CO over H_2 and N_2 for the 5%, 50% and 95% CO compositions tested. A slight selectivity for CO over CH_4 is observed at 5% CO composition due to electrostatic interactions. Also, for CO adsorbing on CuBTC, sorbent-sorbate interactions were shown to dominate over sorbate-sorbate interactions at low loadings as expected. With increasing loading, sorbent-sorbent interactions decreased while sorbate-sorbate interactions increased [29]. In another paper by Karra and Walton, binary mixtures of CO_2, CO and N_2 were tested over four different MOFs including CuBTC and CO_2 was preferentially adsorbed over CO in all the MOFs [30].

Interesting CO adsorption studies have also been done on the surfaces of metal oxides. Though the adsorption environment is different from that inside the pores of a MOF, fundamental interaction knowledge can still be transferred especially at low surface coverages-before pore confinement becomes an issue. Neyman and Rösch used a density

functional density model cluster to investigate the interaction of CO molecules with main group (Mg^{2+}) and transition metal (Co^{2+} and $Ni^{2+)}$ on pure and doped MgO (001) surfaces. They found that for Co^{2+} and Ni^{2+} there was a small but notable π-backbonding interaction while the bonding of CO to MgO was classified as mainly electrostatic [31]. Scarano and co-workers carried out an FTIR study on pure MgO, MgO doped with 10% Ni and Mg doped with 10% Co in order to investigate the role of d-orbital overlap. Since the Ni^{2+} and Co^{2+} ions were diluted in a common MgO, they experienced a common iconicity to Mg^{2+} therefore any observed differences were due to d orbital overlap and not to electrostatic interactions. They concluded that since NiO/MgO frequency was closer to NiO than to MgO, there was some d orbital overlap. Also, the intensity of the Ni^{2+}---CO peak was greater than it would be if only electrostatic interactions were present. Lastly, the frequency of CO on Co^{2+} was lower than on Ni^{2+} which implied a stronger back donation to CO [32].

4.2 Theory

4.2.1 Peng-Robinson Equation

This equation of state (Equation 5) was used to fit the raw experimental data (Appendix C) obtained from the pressure decay system in order to calculate the number of moles of CO adsorbed at each equilibrium pressure. The number of moles was calculated by using Excel solver and initial guesses. The constraint used was that the difference between the right and left side of the equation was zero.

$$P = \frac{RT}{V_m - b} - \frac{a\alpha}{{V_m}^2 + 2bV_m - b^2} \qquad (5)$$

$$a = \frac{0.457235R^2{T_c}^2}{P_c};\ b = \frac{0.077796RT_c}{P_c}; \alpha = \left(1 + \kappa(1 - {T_r}^{0.5})\right)^2; T_r = \frac{T}{T_c}; V_m = \frac{V}{n}$$

$$\kappa = 0.37464 + 1.54226\omega - 0.26992\omega^2$$

P: Pressure

R: gas constant

T: temperature (Kelvin)

V_m: molar volume

a: attraction parameter

b: repulsion parameter

Subscript c: critical

Subscript r: reduced

ω: acentric factor

Table C5 in the Appendix has the list of CO properties needed for Equation 5.

4.2.2 Calculation of Isosteric Heat of Adsorption, q^{st} [22]

To execute this calculation, data were collected at three different temperatures (298K, 313K and 333K). The Clausius-Clapeyron equation (Equations 8a and 8b) was then applied which required ln(P) vs. 1/T at constant loadings. However, there is no way to get identical equilibrium loadings at each temperature as loading was the dependent variable. Therefore, the adsorption loading data (obtained from the Peng Robinson equation calculation) must be fit to an isotherm model. The Toth and Virial isotherm equations were used to do this (Chapters 4.2.2.1 and 4.2.2.2).

It should be noted that this calculation method for q^{st} is very sensitive to errors in measured pressure data therefore derived enthalpies may be unreliable especially in the low surface coverage region [22].

4.2.2.1 Toth Equation (empirical) [33]

The Toth equation reduces to the Langmuir equation when t =1. Therefore t is a measure of surface heterogeneity. Unlike the Freundlich and Sips (Freundlich-Langmuir) equations, the Toth equation appears to give correct limits for both $p \rightarrow 0$ and $p \rightarrow \infty$. It is therefore valid at both the low and high end of the pressure range [33]. Also, although it was originally proposed for monolayer adsorption, it gives a more extensive range of fit when applied to Type I isotherms [22].

$$C_{\mu} = C_{\mu s} \frac{bP}{[1 + (bP)^{t}]^{1/t}} \qquad (6)$$

Cμ: equilibrium loading (mmol of CO/g of MOF)

Cμs: saturation loading (mmol of CO/g of MOF)

P: pressure (bar)

b: parameter (bar^{-1})

t: parameter less than unity

From this equation, Henry's constant is Cμs*b (mmol/g-bar)

4.2.2.2 Virial Isotherm Equation

The Virial isotherm equation, shown in Equation 7, has been successfully applied to noble gases and lower hydrocarbons adsorbed on X-type zeolites. It has the following advantages: (1) the linearity of the plot extends far above the Henry's law limit therefore the evaluation of Henry's constant by extrapolation is more reliable (2) Its application is not restricted to particular mechanisms or systems [22].

$$ln\left({}^{n}/_{P}\right) = B_0 + B_1 n + B_2 n^2 + B_3 n^3 + B_4 n^4 + \ldots\ldots \qquad (7)$$

n: amount adsorbed (mmol of CO/g of MOF)

P: pressure (bar)

B_0, B_1, B_2, B_3, B_4….. characteristic constants for a given gas-solid system and temperature

B_0= ln(H) where H is the Henry's constant

4.2.2.3 Clausius-Clapeyron Equation

Once the data were fit and all the parameters solved for ($C_{\mu s}$, b, and t for the Toth equation and B_0, B_1, B_2, B_3, B_4….. for the Virial isotherm equation) with the aid of Origin software, the pressures corresponding to a chosen set of loadings were calculated. For the Toth equation, these pressures were predicted using excel solver. Initial guess pressures were chosen and the solver criteria were that $P \geq 0$ and that the difference between the calculated loadings and the specified loadings was zero. For the Virial isotherm equation, solver was not needed as ln(P) could be calculated directly from the known parameters and specified loadings. Ln(P) was needed for the Clausius-Clapeyron equation (Equation 8b) in order to calculate q^{st}. Note that in this case, $\Delta H = q^{st}$ and the assumption that it is independent of temperature is used.

$$\frac{d\ln P}{dT} = -\frac{q^{st}}{RT^2} \qquad (8a)$$

$$\frac{dlnP}{d(1/T)} = -\frac{q^{st}}{R} \qquad (8b)$$

P: vapor pressure

T: temperature (Kelvin)

q^{st}: isosteric heat of adsorption (J/mol)

R: gas constant (J/mol-K)

4.3 Results and Discussion

All experimental methods including MOF synthesis procedures were described in Chapter 2.

The nitrogen adsorption data on the MOF-74 materials used for the carbon monoxide studies are shown in Table 6. The magnesium and nickel MOFs were from a different batch than those used for the water studies because there was not enough material left over. Notably, their surface areas seem a bit low and a bit high respectively in comparison to the previous batches and also to the literature values.

Table 6. Nitrogen Sorption Data for As-Synthesized Samples

Material	Measured Surface Area/m^2		Activation Conditions
	Samples	Previously Reported	
Mg-MOF-74	1166	1206[a]; 1495[c]	200°C for 5 hours
Zn-MOF-74	842	496[a]; 632[b]; 816[d]	150°C overnight in vacuum oven and then at 200°C for a few hours
Co-MOF-74	984	835[a]; 1080[c]	150°C overnight
Ni-MOF-74	1159	599[a]; 1070[e]	250°C overnight in vacuum oven and then at 250° on activation station for a few hours

a- ref[6]; b-ref[17]; c-ref[2]; d-ref[18]; e-ref[7]

4.3.1 CO Adsorption Isotherms

Figures 12 to 14 show the CO loadings for all four isostructural MOFs at 298, 313, and 333K respectively (25, 40 and 60˚C). All the isotherms are of Type 1 indicative of the MOFs' affinities for CO, especially in the case of the cobalt and nickel isostructures. As expected, as the temperature increases, the maximum loading decreases. At 298K and P < 4 bar, the loading of CO follows the order Co-MOF-74>Ni-MOF-74>Zn-MOF-74>Mg-MOF-74 except for a small initial overlap region for nickel and cobalt. Above 4 bar, Zn-MOF-74 surpasses Ni-MOF-74 in loading. This is at first counterintuitive due to the fact that the zinc MOF has a lower surface area than the nickel MOF (see Table 6) but can be rationalized by the fact that for Zn-MOF-74, dispersion accounts for 2/3 of its total binding whereas it only accounts for ½ the total binding for Mg-MOF-74 and Ni-MOF-74, as discovered by Valenzano et al [34]. Co-MOF-74 was not examined. Higher pressures are synonymous with higher loadings therefore the primary binding sites (open metal sites) would already be filled and dispersion would factor into any remaining

attraction to the adsorbent pore surface and into attraction between adsorbate-adsorbate molecules.

The low pressure trend is the same for the isotherms collected at 313K except for the fact that Co and Ni are coincident up to slightly higher pressures. Above 4 bar this trend remains the same so the zinc never supersedes nickel, though the shape of it implies that it would have if higher pressures were tested.

Lastly, at 333K, Ni-MOF-74>Co-MOF-74 up to about 0.5 bar but this order reverses before 1 bar is reached and remains that way for all higher pressures with zinc and magnesium having the 2nd lowest and lowest loadings respectively. Overall it should be noted that Ni-MOF-74 does not change as much with temperature as do the other MOFs. This point will be referred to again in later discussions about isosteric heat of adsorption and Henry's constant.

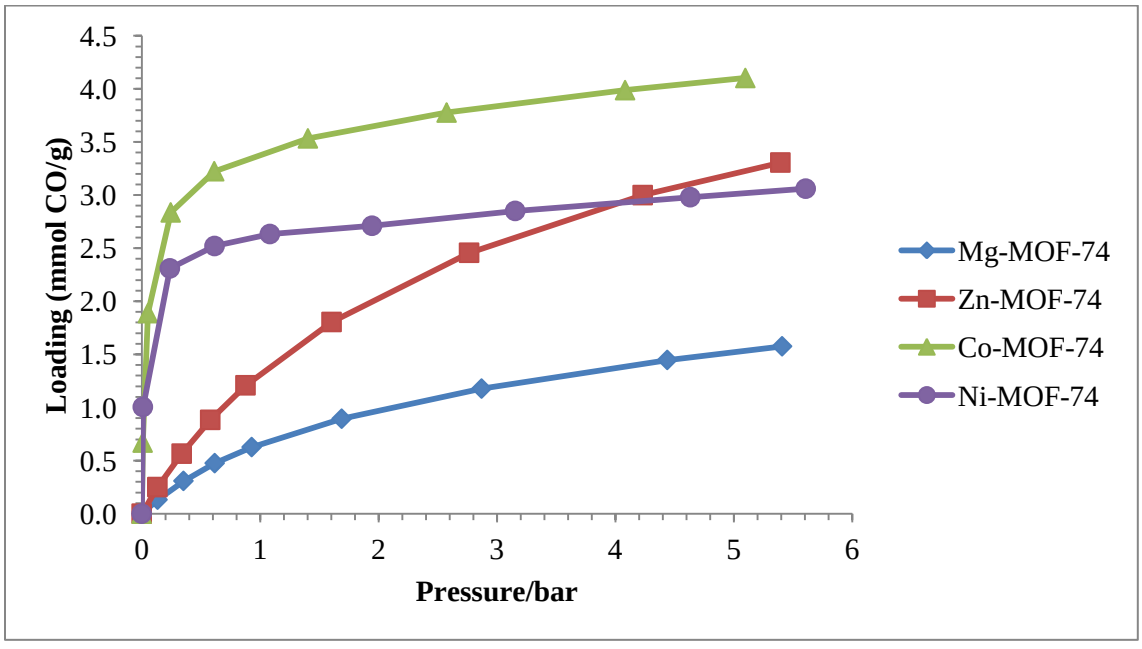

Figure 12: CO Adsorption Isotherms at 298K

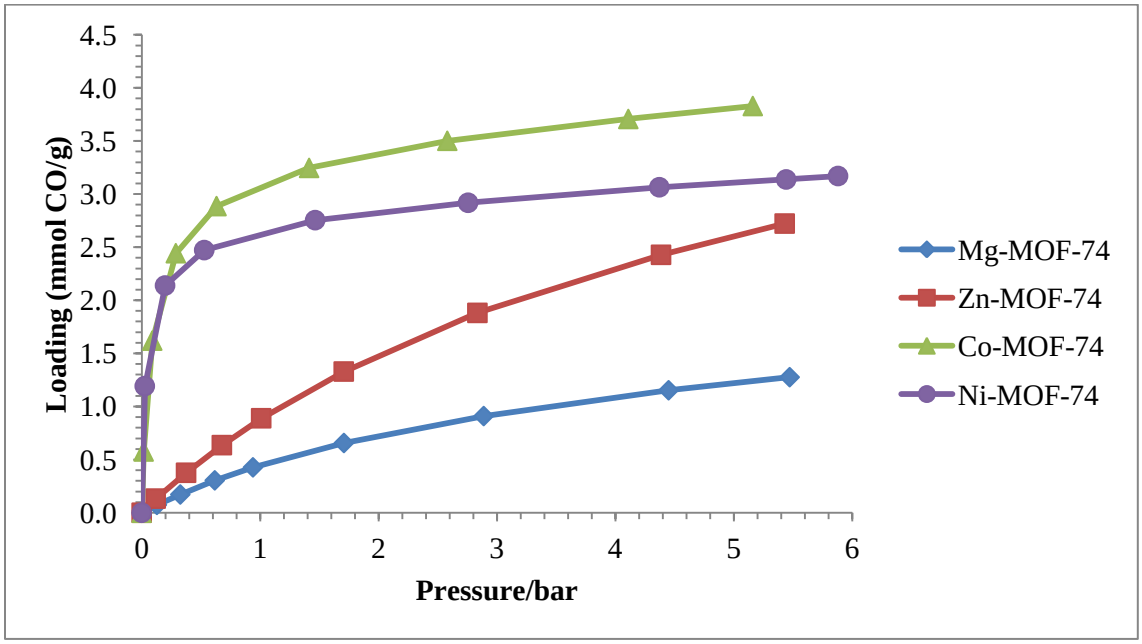

Figure 13: CO Adsorption Isotherms at 313K

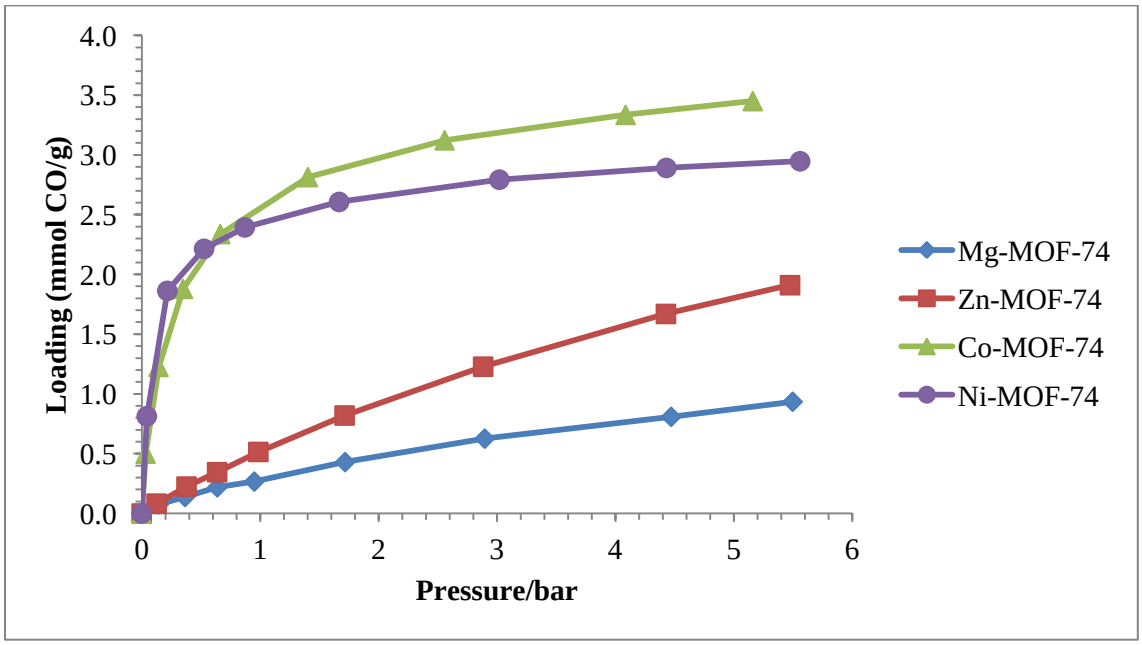

Figure 14: CO Adsorption Isotherms at 333K

Note that for the water studies, Mg-MOF-74 had the highest loading at 298K and 1 bar (Figures 3 and 8) especially at lower relative humidities but for CO it has the lowest loading under similar conditions and also for all tested conditions. This makes sense since metal-adsorbate interactions dominate in the low pressure regions and water and CO have very different properties. Water is a hard Lewis base (excellent sigma donor) and CO is a poor sigma donor (Lewis base) and a very strong π acceptor. When carbon monoxide bonds to a metal it bonds through two processes. The first process involves the donation of the lone pair on carbon atom into a symmetry-matched vacant *d*-orbital on the metal; this electron donation increases the electron density on the metal. The second process is π-backbonding (or π-backdonation) and this compensates for this increased electron density and hence stabilizes the coordination complex because a filled symmetry-matched metal *d*-orbital interacts with the empty π* orbital on the carbon (Figure 15) [35]. In order for π-backbonding to occur, *d* orbitals are needed.

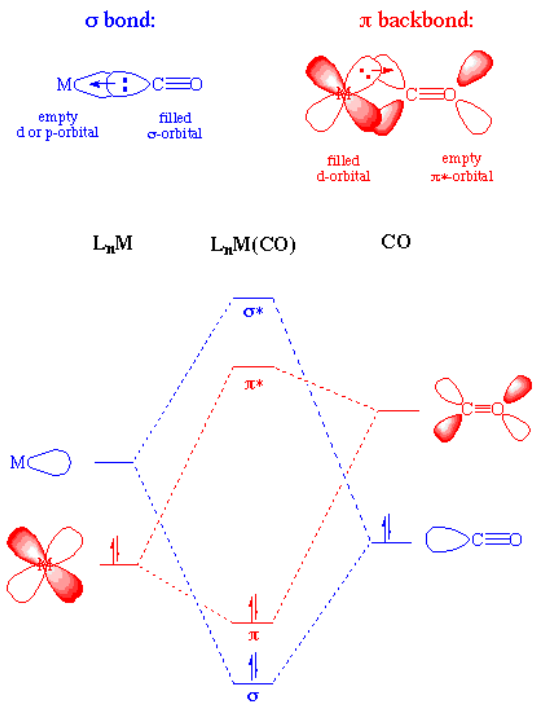

Figure 15: Two Types of Bonding Involved When CO Binds to a Metal. Figure taken from [35]

Mg-MOF-74 therefore has the lowest loading of CO because it does not have any *d* orbitals to take part in π- backbonding. The Zn^{2+} metal has ten *d* electrons, Co^{2+} has eight and Ni^{2+} has seven. The increased loading of CO for Co-MOF-74 over Ni-MOF-74 outside of the extremely low pressure range is based on the periodic trend in orbital energies: In going from left to right across the periodic table, the *d* orbital potential energies decrease (drops lower on diagram) introducing a bigger difference between the potential energies of the metal d_π and the CO π* orbitals (See Figure 15) such that these orbitals are now less energetically matched with each other resulting in weaker interactions between them. As a result, the π-backbonding orbital interaction becomes

worse [36]. It is reasonable then that Zn-MOF-74 has a lower loading than both the nickel and cobalt versions.

At 298K, Ni-MOF-74 and Co-MOF-74 have higher CO loadings at 1 bar than zeolite 5A, zeolite 13X , MOF-5 and MOF-177 while Zn-MOF-74 has about the same loading as zeolite 5A but surpasses the three other tested materials [28]. Also, Van't Hoff plots of Henry's constant versus 1/T reveals that CO adsorbs more strongly on zeolite 5A than it does not zeolite 4A [37]. Therefore zeolite 4A is no match for the nickel and cobalt isostructures

From the data from Lopes and coworkers, all of the MOF materials tested here, except perhaps the magnesium isostructure, out-perform activated carbon based on the fact that at 303K (only 5K higher than the temperatures used in these experiments), the loading is less than 0.5 mmol/g [38]. Grande and co-workers got a slightly higher value for activated carbon of about 0.7 mmol/g which again is outperformed by the cobalt and nickel isostructures and perhaps also by the zinc isostructure [39].

Also, compared to experimental CO data collected on CuBTC by Wang and co-workers at 295K and also simulation data collected by Karra and Walton, all of the MOF-74 materials except magnesium have higher loadings than CuBTC at 1 bar [29, 40]. Since the temperature difference is only 3K, this comparison is reasonable. Data collected by Chowdhury and co-workers gave a slightly higher loading for CuBTC under these

conditions (1.4 mmol/g versus 0.8 mmol/g) which, in comparison to the data collected here, is comparable to Zn-MOF-74 but surpassed by both Ni- and Co-MOF-74 [41].

In conclusion, to the best of my knowledge, Co-MOF-74 has the highest CO loading at 298K and 1 bar to date. Table 7 has a comparison of CO loadings for reported microporous materials at 298K and 1 bar. These values were read of from isotherms plots hence the word "approximate" in the table. It should be noted that when comparing MOFs not in the same isostructural family, other factors besides the identity of the open metal site need to be considered e.g. pore geometry and dimensionality.

Table 7. Comparison of MOF-74 CO Loadings with Other Microporous Materials

Microporous Material	Approximate Adsorption Loading at 1 bar & 298K (mmol CO/g)
Co-MOF-74	3.35
Ni-MOF-74	2.6
Zn-MOF-74	1.3
Zeolite 5A (CaA)	1.25 [28]
CuBTC	0.8; 1.4 (295K) [38, 39]
Mg-MOF-74	0.65
Zeolite 13X (NaX)	0.5 [28]
Activated carbon	0.5; 0.7 (303K) [40, 41]
MOF-5	0.15 [28]
MOF-177	0.1 [28]

4.3.2 Number of Molecules per Unit Cell

As was done in section 3.2.3., both the N_2 sorption data and the CO data were converted into number of molecules per unit cell to account for the weight effect (Table 8 and Figures 16 to 18) in order to see if there is indeed an effect based on metal identity and not weight.

Table 8. Number of N_2 Molecules per Unit Cell for MOF-74 Materials Used in CO Experiments

Material	BET Surface Area (m^2/g)	Number of N_2 Molecules per Unit Cell
Mg-MOF-74	1166	26.1
Zn-MOF-74	842	25.2
Co-MOF-74	984	28.3
Ni-MOF-74	1159	33.3

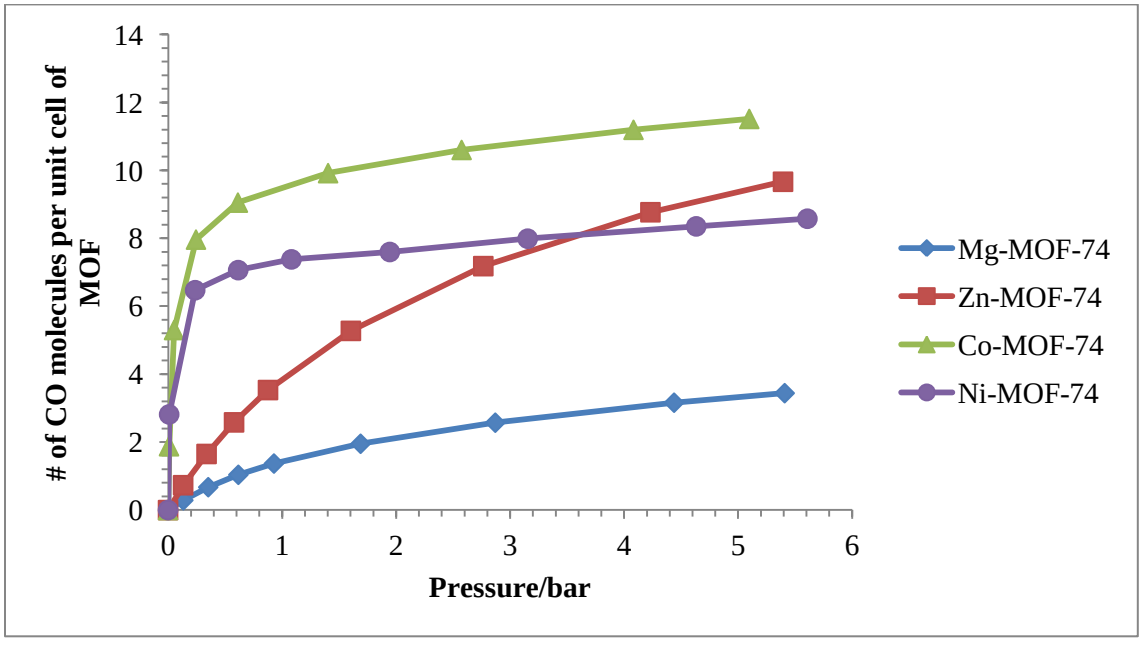

Figure 16: Number of CO Molecules per Unit Cell at 298K

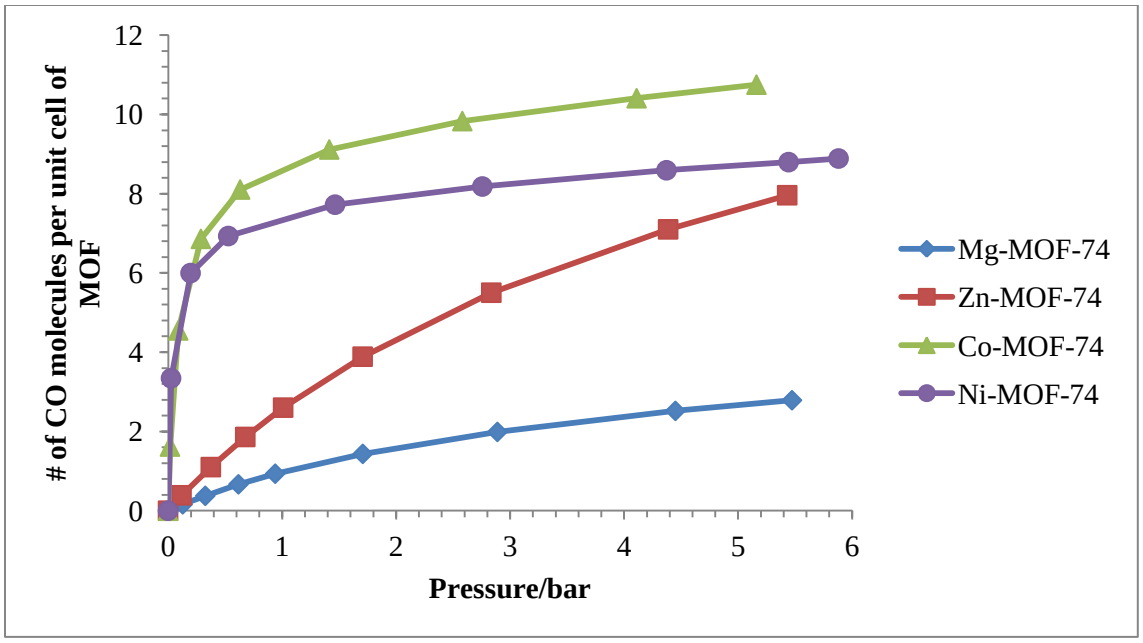

Figure 17: Number of CO Molecules per Unit Cell at 313K

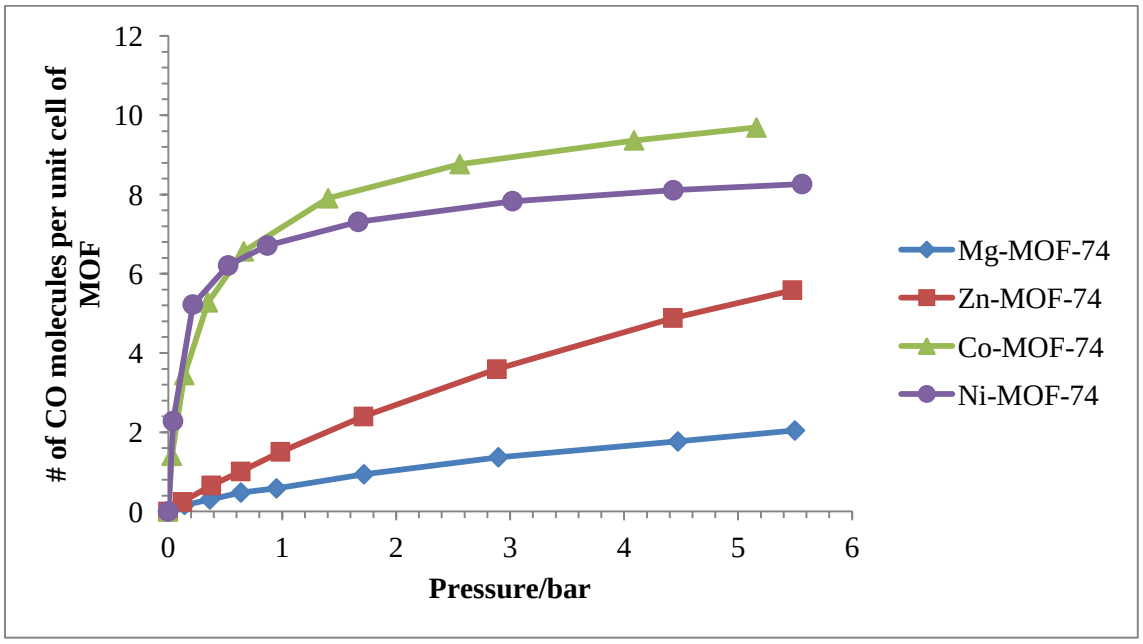

Figure 18: Number of CO Molecules per Unit Cell at 333K

Similar to the observations with the water data it should be noted that once the weight effect is removed, there are still differences observed for the different metals for both the N_2 and CO adsorption data. In fact, the graphs of CO adsorption look almost identical with and without consideration of the weight effect. Thus, there is definitely some interaction that depends solely on the metal involved.

4.3.3 Heat of Adsorption Data

A quantum mechanical study on a MOF-74 sequence of materials (Mg, Ni, Zn), referred to as CPO-27 in the paper by Valenzano and coworkers, predicted different sequences of binding energies (heats of adsorption at zero coverage) for CO as compared to CO_2 . Binding energies indicate the strength of adsorbent-adsorbate interactions. For CO, the sequence was Ni>Mg>Zn and for CO_2 the sequence was Mg>Ni>Zn [34]. Co-MOF-74 was not included in the study. Their simulations revealed that dispersion accounts for at least half of the binding energies for both CO and CO_2.

The results obtained here for CO isosteric heats of adsorption obtained via the Toth and Clausius-Clapeyron equations showed the sequence: Ni>Mg > Zn (Figure 19) in agreement with Valenzano and coworkers. From the adsorption curves, the loading sequence is Ni>Zn ≈Mg for P < 0.2 bar (towards zero loading) at 298K. At the higher, temperatures, the loading sequence is Ni>Zn>Mg. Therefore the adsorption isotherms don't quite match the observed q^{st} at very low loadings for 298K. As an aside, the aforementioned CO_2 binding energy sequence obtained by Valenzano et al. agrees well with Caskey et al.'s initial affinity results for CO_2 which also included Co-MOF-74; the

sequence obtained was Mg>Ni>Co. Heat of adsorption calculations were not done for the zinc isostructure and no experiments were carried out using CO.

With the exception of Mg-MOF-74 and Zn-MOF-74, the isosteric heats of adsorption, q^{st}, obtained from the Toth equation isotherm model are considerably different from those obtained from the Virial equation model (Table 9 and Figures 19 to 21) even though both isotherm equations, model the adsorption data well except for the Virial fit for Ni-MOF-74 at 298K (see Figures in Appendices E and F). In terms of reported literature values, the q^{st} literature value for Mg-MOF-74 was obtained from variable temperature IR spectroscopy and the q^{st} literature value for Ni-MOF-74 was obtained from calorimetry. Reported q^{st} values were only found for Mg- and Ni-MOF-74 and the values obtained for Mg-MOF-74 match well with literature.

Table 9. Comparison of q^{st} Obtained From Toth and Virial Isotherms to Literature Values

Material	q^{st} Values Derived from Toth Isotherm (kJ/mol)	q^{st} Values Derived from Virial Isotherm (kJ/mol)	q^{st} Literature Values (kJ/mol)
Mg-MOF-74	~29	~27	29 [27]
Zn-MOF-74	28-26	27-28	-
Co-MOF-74	58-66	29-48	-
Ni-MOF-74	85-101	893-4	55[23]

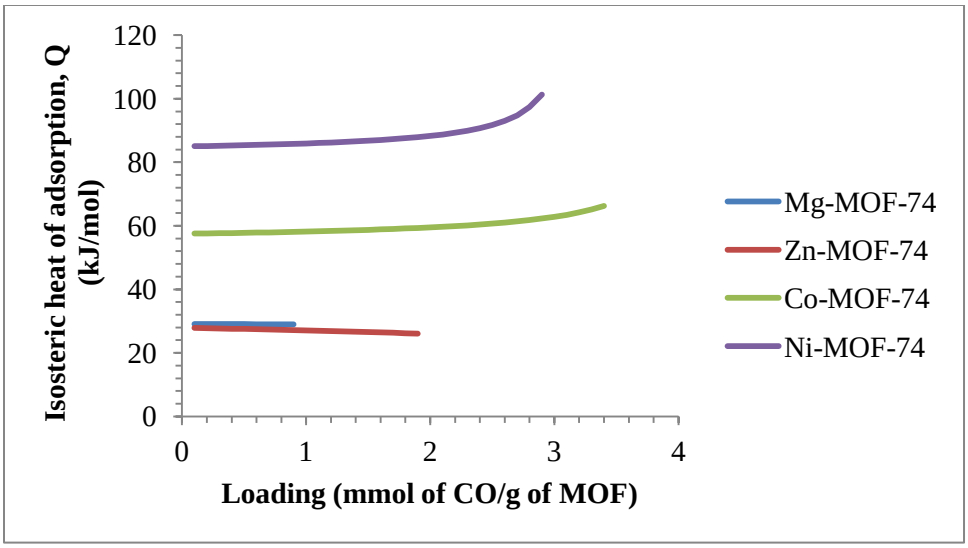

Figure 19: Heat of Adsorption Versus Loading for all Four MOFs Fitted with the Toth Isotherm

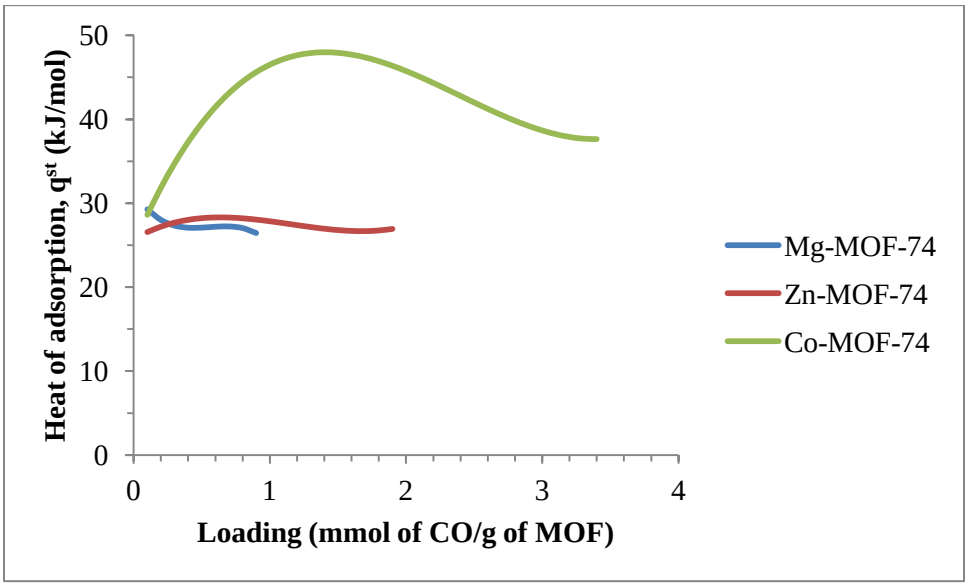

Figure 20: Heat of Adsorption Versus Loading for all Four MOFs (Except Ni) Fitted with the Virial Isotherm

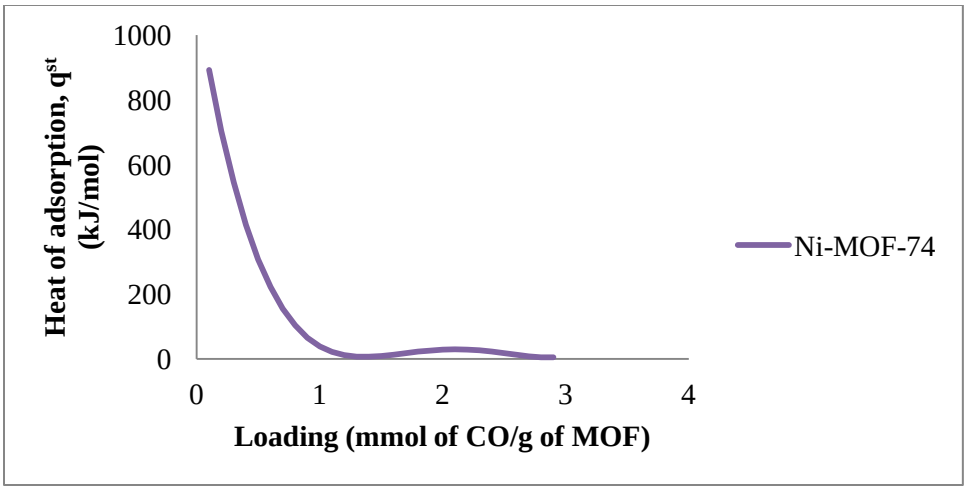

Figure 21: Heat of Adsorption Versus Loading for Ni-MOF-74 Fitted with the Virial Isotherm

From the Toth-derived results, it can be seen that isosteric heat, q^{st}, is constant with respect to loading for Mg-MOF-74 but decreases slightly for Zn-MOF-74 with increased loading. For both Co- and Ni-MOF-74, isosteric heats increase as a function of loading. The q^{st} values obtained for Ni-MOF-74 are higher than the reported literature value and high enough that chemisorption is suspected. However, this cannot be proven or disproven with the limited data shown here.

In the case of Mg-MOF-74, the constant isosteric heat is indicative of the adsorbent-adsorbate interaction decrease being matched by an equivalent increase in adsorbate-adsorbate interactions. It can also be indicative of an energetically homogeneous surface. A homogeneous surface is characteristic of a Langmuir-type surface and it implies that adsorption energy is constant over all sites [33]. The surface inside the Mg-MOF-74 is known to be locally heterogeneous but globally may in fact be homogeneous.

The trend observed for zinc was expected for all four MOF-74 compounds because it implies that the interaction with the most favorable sites (open metal sites) occurs first and once these sites are saturated, less favored adsorbate-adsorbate interactions take place; however, this is not the case.

The trend of increasing isosteric heat with increasing loading for the nickel isostructure is unexpected and implies that (1) some of the data collected for this MOF did not reach equilibrium and/or that (2) the Clausius-Clapeyron equation may not be able to accurately model its isotherms. The first point refers to the fact that the CO isotherm for Ni-MOF-74 at 298K does not have the highest loadings when compared to the other isotherms collected at 313 and 333K (Figure 22). Notably, another Ni-MOF-74 sample from another batch was tested and this same observation was made so it may not be an experimental error. The second point refers to the fact that the ln(P) versus 1/T plot needed for the Clausius-Clapeyron equation (the slope of which is used to calculate q^{st}) is not at all linear for nickel (Figure 23). This could be due to the fact that the nickel isotherms don't vary as much with temperature as do the other isotherms, as alluded to previously. In light of these observations, Ni-MOF-74 isotherms should therefore be modeled using other isotherm models and a different method of calculating q^{st} should be used for comparison.

Co-MOF-74 also shows that q^{st} increases with increased loading but this increase is less dramatic than its nickel counterpart and abnormalities in the isotherms and the ln(P) versus 1/T plots are not observed. The isotherms done in this work should be repeated to

ensure accuracy and, as with the nickel isostructure, other isotherm models and methods of calculating q^{st} should be explored. Although unexpected, it is possible for q^{st} to increase as loading increases. For example, Karra and Walton calculated the isosteric heats of adsorption as a function of loading for CO adsorbed on CuBTC and they showed a slight increase in q^{st} as a function of loading after an initial decrease [29].

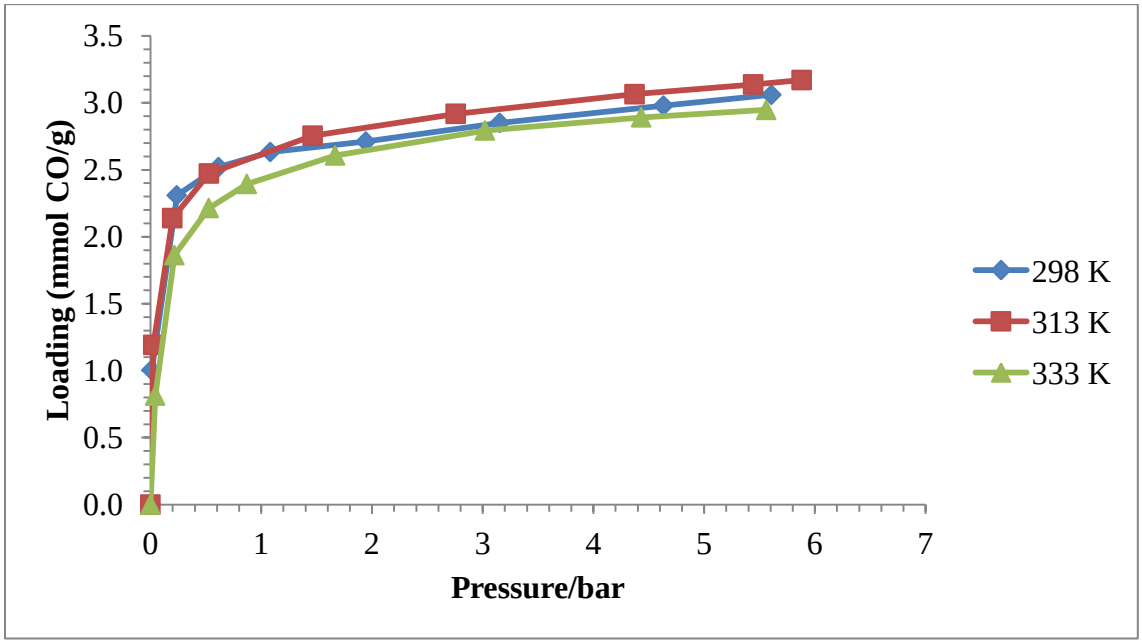

Figure 22. Comparison of CO Isotherms for Ni-MOF-74 at 298, 313, and 333K

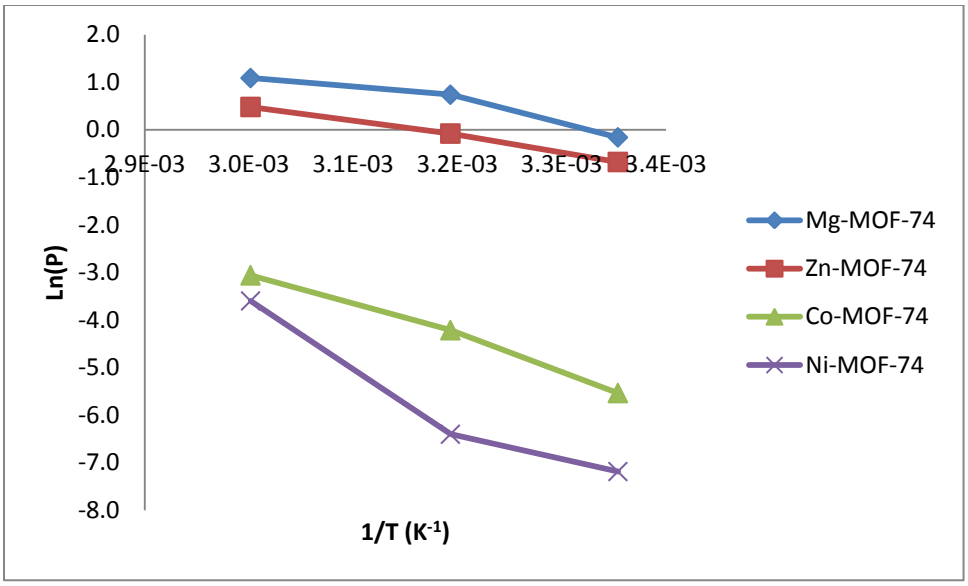

Figure 23. lnP vs. 1/T for MOF-74 Compounds at 0.9 mmol CO/g Loading from the Toth Equation Results

All of the isosteric heats obtained from the Virial isotherm data-fit show inflection points which give the q^{st} curves an unusual undulating characteristic. For Mg-MOF-74 it shows a gradual decrease of q^{st} with increased loading and not the independence with loading that the Toth equation predicted. For zinc, the undulation observed is slight and shows q^{st} increasing and then deceasing with loading. For Co- and Ni-MOF-74, the q^{st} curves are nonsensical and therefore the Virial isotherm equation is clearly not suitable for modeling the isotherm data for these isostructures. This is especially so for Ni-MOF-74 since, as mentioned previously, it fails to model the 298K data accurately (Appendix F). Also, as was the case for the Toth isotherm equation, the plot of ln(P) versus 1/T required for use of the Clausius-Clapeyron equation, is non-linear for this MOF again suggesting that this equation is probably not be an accurate way of determining q^{st} for this isostructure (Figure 24) due to the isotherms not varying much with temperature.

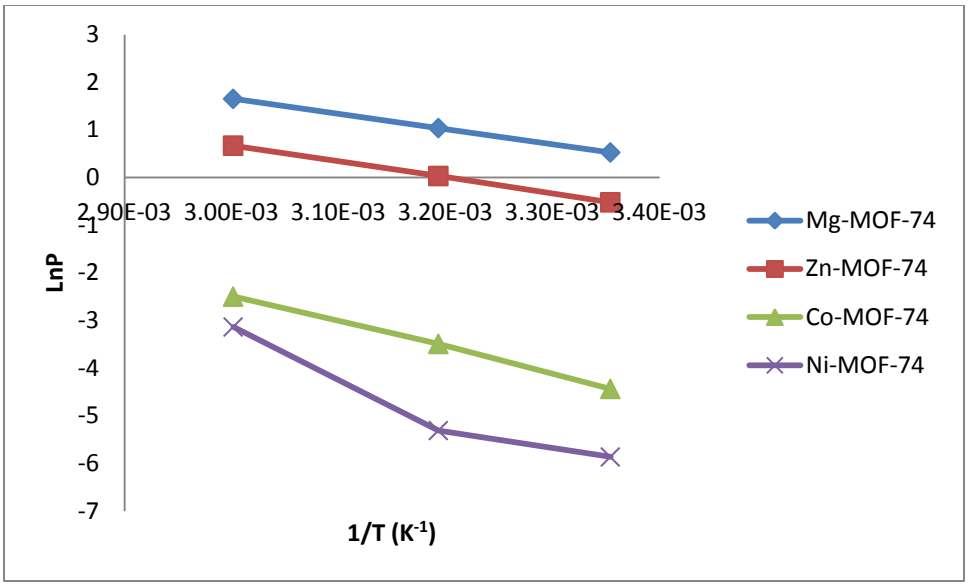

Figure 24. lnP vs. 1/T for MOF-74 Compounds at 0.9 mmol CO/g Loading from the Virial Equation Results

In terms of Co-MOF-74, it is a bit surprising that the Virial isotherm equation appears unable to accurately model the data even though it fits the data quite well (Appendix F). However, the unusual q^{st} curves obtained for both Co- and Ni-MOF-74 can be partially rationalized by the discovery about the Virial isotherm that it can only be used if the isotherm curvature is not too great [22]; this of course excludes both Co- and Ni-MOF-74.

In fitting the data using the Virial isotherm equation, a 2^{nd} order form of the equation was used for Mg-MOF-74, a 3^{rd} order form was used for Zn- and Co-MOF-74 and a 4^{th} order form was used for Ni-MOF-74. These polynomial choices were based on the level of fit that could be obtained and whether or not the calculated pressures for chosen loading values made sense. If a higher order polynomial did not provide reasonable

improvement for the fit and the equation parameters, it was not used. Refer to Appendix F for the tabulated Virial constants.

It should be noted that for both the Toth and Virial data fits, the first three loadings for Mg-MOF-74 at 333K were not included. This was done for the Toth because the solution would not converge and for the Virial for consistency. In fact, from Figure 14, an unusual dip in the 333K isotherm can be observed for Mg-MOF-74 over the first few points. This may have been due to equilibrium not being reached for all of these points. Notably though, at this higher temperature, the water bath, in which the pressure decay system was submerged, had a more difficult time maintaining constant temperature due to the air currents in the fume hood and from the raising and lowering of the fume-hood sash.

4.3.4 Henry's Constants

The Henry's constants for each material at each of the different temperatures calculated using both the Toth and the Virial isotherm models are shown in Table 10. The Henry's constant is obtained from the extrapolation of adsorption at zero coverage and is therefore a criterion for affinity of adsorption at low surface coverages [22]. In other words, it gives information about the adsorbent-adsorbate interactions. Adsorbate-adsorbate (lateral) interactions need not be considered because adsorbate molecules are at infinite dilution in the Henry's law region. Also, the amount adsorbed is linearly related to pressure.

Table 10. Henry's Constants (mmol/g-bar) for MOF-74 Materials at 298, 313, and 333K for Both Toth and Virial Equations

		Mg-MOF-74	Zn-MOF-74	Co-MOF-74	Ni-MOF-74
Toth	298K	1.39	2.08	283.9	1608
	313K	0.632	1.14	77.0	715
	333K	0.399	0.635	24.6	50.0
Virial	298K	1.10	2.06	73.5	1.14E20
	313K	0.595	1.18	40.4	7.97E9
	333K	0.346	0.690	25.3	0.299

The Henry's constant decreases with increased temperature for all the MOFs and from the Henry's constants obtained from the Toth equation (Table 10), Ni-MOF-74 has the greatest affinity for CO at low surface coverages. From the three isotherms collected, this is most apparent in the low coverage region of the 333K adsorption isotherm (Figure 15) where the loading for Ni-MOF-74 is higher than for Co-MOF-74. Due to Ni-MOF-74 having the highest affinity at low coverages it also has the highest isosteric heat at these low coverages as expected (Figure 19). After Ni-MOF-74, Co-MOF-74 has the highest affinity followed by Zn- and Mg-MOF-74 respectively. Based on the fact that at the lowest loadings, q^{st} for Mg-MOF-74 is higher than Zn-MOF-74 (Figures 19 and 20), I expected Zn-MOF-74 to have the lowest Henry's constants.

The Henry's constants obtained from the Toth and Virial isotherm equations for the cobalt and nickel isostructures are indicative of such high affinities that chemisorption seems to be a strong possibility but, as already stated, cannot be conclusively determined without further investigation. Ni-MOF-74's superior affinity for CO over Co-MOF-74 at low coverages is actually a bit surprising because Co^{2+} undergoes more π-backbonding

that Ni^{2+} as observed by Scarano et al. in their FTIR studies on Co^{2+} and Ni^{2+} exposed on the surface of a doped MgO matrix [32]. This conclusion came because the frequency of CO on Co^{2+} was lower than on Ni^{2+}. Pi-backbonding strengthens the bond between CO and the metal but weakens the bond between the C and O of the CO molecule. The reason for the superior affinity may therefore be due to increased electrostatic interactions and/or possibly also magnetic interactions but this needs to be investigated further.

From the Virial isotherm, only the Henry's constants obtained from Mg-MOF-74 and Zn-MOF-74 are considered accurate because, as already explained, the Virial isotherm fails to model nickel and cobalt accurately. This is reinforced by the outrageous Henry's constant values obtained for nickel.

4.4 Conclusions

At 298 K and 1 bar, Co-MOF-74 has the highest CO loading reported thus far- 2.5 times as much as zeolite 5A which was the previous highest under these conditions. The observed trends in CO loading for the MOF-74 materials are a result of pi-backbonding that occurs when CO binds to a metal center and the metal subsequently donates some electrons from its *d* orbital to the empty π* orbital on CO, stabilizing the metal-CO complex. Mg has the lowest loading because it has no *d* orbitals to participate in π backbonding and the other loadings follow the general trend of Co>Ni>Zn because the *d* orbital energies decrease in that order and therefore π-backbonding also decreases. Zn-MOF-74 has a greater loading than Ni-MOF-74 at 298K at P > 4 bar and 298K because dispersion accounts for 2/3 of its total forces in comparison to only ½ for the other

MOFs. Without the weight effect, the number of molecules per unit cell for nitrogen sorption and for CO is different for each metal so there are definitely some metal effects to consider.

According to the Toth equation, q^{st} for Mg-MOF-74 is constant with respect to loading but decreases gradually with loading when the Virial equation is used. Independence of q^{st} with respect to loading implies that the decrease in the adsorbent-adsorbate interactions are balanced by the increase in adsorbate-adsorbate interactions or that globally the pore surface is homogeneous. For Zn-MOF-74, the Toth-based results show that q^{st} decreases with increased loading while it increases and then decreases with the Virial equation. In the case of Co- and Ni-MOF-74, q^{st} increases with increased loading for the Toth-based results. These qst values are so high that chemisorption is suspected but further investigation is required. The Virial-based results for the cobalt and nickel isostructures are nonsensical which stems from the fact that the Virial equation is not capable of modeling isotherms with very sharp knees. Consequently, the Toth equation can model the data better overall and is therefore the more reliable model.

For Ni-MOF-74 it is believed that Clausius-Clapeyron equation cannot be used to accurately determine q^{st} and other methods should be used, for example calorimetry. For Co-MOF-74 the isotherms should be repeated to confirm the observed trend. The use of different isotherm models is also recommended for both of these isostructures. Finally, the Henry's constants for the MOFs are somewhat consistent with the low coverage q^{st}

curves as expected, with the highest interaction observed for Ni-MOF-74. The remaining MOFs follow the trend Co>Zn>Mg but a trend of Co>Mg>Zn was expected.

CHAPTER 5

SUMMARY, CONCLUSIONS, RECOMMENDATIONS FOR FUTURE WORK

5.1 Summary and Conclusions

As hypothesized, it is possible to investigate the effect of varying the metal by using an isostructural family of MOFs, where the only difference from one MOF to the other is the identity of the metal incorporated into the framework. This was clearly demonstrated by the fact that when the weight effect was removed by the calculation of number of molecules per unit cell, differences between isostructures persisted.

The loadings for water and CO have different trends, most importantly in the low pressure region where the metal-adsorbate interactions dominate. For water at 298K and 1 bar, the trend was Mg-MOF-74>Zn-MOF-74>Co-MOF-74>Ni-MOF-74 and for CO the trend at 1 bar and over the tested pressure range was Co-MOF-74>Ni-MOF-74>Zn-MOF-74>Mg-MOF-74 except at pressures less than 0.5 bar at each tested temperature. This is because in the case of water, the determining factor was the degree of Lewis acidity of the open metal site whereas for CO the determining factor was the extent of π-backbonding. From the literature data found, Co-MOF-74 has the highest CO loading to date of any microporous material at 1 bar and 298K.

Both the water study and the CO studies are fundamentally important since many gas separation processes for which MOFs are potential applications involve humid streams which mandate the maintenance of MOF structural integrity for prolonged use. Unfortunately, none of the four MOFs in this isostructural family retain their full structural integrity on exposure to humidified air streams due to microstrain and/or exposure to oxygen but they can still be regenerated and reused to some extent as proven by Kizzie et al. Whether or not the MOF can be stored under a normal atmosphere and for how long can also be determined. In addition, CO studies are quite rare in the literature but quite essential since it is an unwanted impurity in some industrial processes such as steam reforming and coal gasification and can be deadly on exposure to high enough concentrations.

The Toth isotherm provides a better fit for CO data on the MOF-74 materials than the Virial isotherm, which can only appropriately model the magnesium and nickel MOFs. From the Toth equation results, q^{st} is constant, decreases and increases for Mg-, Zn- and Co- and Ni-MOF-74 respectively. In addition, Henry's constant calculations reveal that Ni-MOF-74 has the highest affinity for CO.

Ni-MOF-74 has the lowest water loadings and the highest CO loadings at extremely low partial pressures. Therefore, of all of the tested MOFs in this series, it shows the most promise for removing CO from humid streams containing very low partial pressures of CO. Despite its clear structural collapse via PXRD, it has been shown to be successfully regenerated and reused in the case of CO_2 humid streams [9, 11]. Admittedly,

selectivities cannot be directly inferred from pure component isotherms but they can provide a qualitative sense of what gas will be preferred over the other.

Because the kinetic diameter of H_2O (2.64 Å) is so much smaller than the kinetic diameter for CO (3.69 Å), the MOF-74 materials have a much higher capacity for water than they do for CO since more molecules can fit into the pore space [42]. This is especially emphasized by the number of molecule per unit cell values (Figures 11 and Figures 16 to 18).

5.2 Recommendations for Future Work

5.2.1 H_2O Study

For the water study, a detailed variable temperature PXRD study should be carried out on Mg- and Ni-MOF-74 to examine the dehydration process more closely as was done with Zn- and Co-MOF-74 by Dietzel and co-workers [19]. This study should also be done on the rehydration of all four isostructures. In addition, an elemental analysis technique such as TGA/MS should be performed on the MOF samples after exposure to the humidified stream to see what decomposition products are being released and at what temperatures.

5.2.2 CO Study

Adsorption isotherms should be re-collected for Co-MOF-74 and for Ni-MOF-74 especially. Also, other isotherm models should be used to model the data obtained for all

the MOFs to see if the same trends are obtained. An example of a model that can be used is the Sips (Langmuir-Freundlich) equation which has actually been used by Chavan and co-workers to model the adsorption of CO on Ni-MOF-74 at pressures below 0.1 bar [23]. Also, another method of calculating q^{st} should be used for all the MOFs especially for Ni-MOF-74; one such method is calorimetry. Since chemisorptions is possible for Co- and Ni-MOF-74, desorption isotherms should be collected and the gas desorbing should be tested for possible reaction products.

IR measurements should also be done to investigate stretching frequencies due to the abundance of literature available. Pi-backbonding weakens the bond between the carbon and the oxygen of the carbon monoxide molecule and therefore a lower stretching frequency is observed when more π-backbonding is present. More specifics about the CO binding nature (e.g. whether linear or bridged) can also be obtained via this method. In addition to IR spectroscopy, XRD on the CO-containing MOF can be obtained and the structure can be solved in order to locate exactly where the CO atoms are inside of the MOF.

5.2.3 General Recommendations

Once the aforementioned recommendations have been completed, some other members of the isostructural family of MOFs (Mn, Fe, Ca, and Sr) should be tested [20, 43, 44]. For the water adsorption data, the predicted trend is Mg-MOF-74> Ca-MOF-74>Sr-MOF-74>Mn-MOF-74>Zn-MOF-74>Co-MOF-74>Ni-MOF-74>Fe-MOF-74. This prediction is based on the qualitative HSAB (Hard Soft Lewis Acid Base) theory. Since

each metal has the same +2 charge, the determining factor is the size of the metal cation and the atomic electronegativity. According to Zhang's quantitative values of Lewis acidity for the ions involved, the trend would be Ca-MOF-74>Sr-MOF-74>Mg-MOF-74>Zn-MOF-74>Fe-MOF-74>Co-MOF-74>Mn-MOF-74>Ni-MOF-74 [15]. Table 11 gives relevant ionic radii atomic electronegativities and Lewis acid strength values. Notably, Mn has an unexpectedly low electronegativity that is within the range of electronegativities for hard Lewis acids (0.7-1.6) [45].

Table 11. Ionic Radii of Divalent Cations and the Electronegativities of Their Corresponding Neutral Atoms

Cation	Ionic Radius/Å [14]	Electronegativity (Dimensionless Pauling Scale)	Lewis Acid Strength[15]
Ca^{2+}	1.0	1.0	1.593
Sr^{2+}	-	0.95	1.417
Mg^{2+}	0.72	1.31	1.402
Zn^{2+}	0.74	1.65	0.656
Fe^{2+}	0.78	1.83	0.390
Co^{2+}	0.75	1.88	0.356
Mn^{2+}	0.83	1.55	0.307
Ni^{2+}	-	1.91	0.293

For CO adsorption data, the predicted trend is Mn-MOF-74>Fe-MOF-74>Co-MOF-74>Ni-MOF-74>Mg-MOF-74>Ca-MOF-74>Sr-MOF-74. This is based on π-backbonding arguments: Mn^{2+}, Fe^{2+}, Co^{2+} and Ni^{2+} are all in the same row of the periodic table so their d orbital energies decrease towards Ni^{2+} therefore less energetic overlap can occur with CO π* orbitals and therefore less π-backbonding. Mg^{2+}, Ca^{2+} and Sr^{2+} all lack d-orbitals to participate in backbonding . Therefore if there are differences in their loadings, this would be due to electrostatic interactions with the CO molecule.

APPENDIX A

POWDER XRD DATA FOR SIMULATED VS. AS-SYNTHESIZED DATA FOR MOF-74 MATERIALS USED IN H_2O AND CO EXPERIMENTS

MOF-74 Materials used in H_2O Experiments

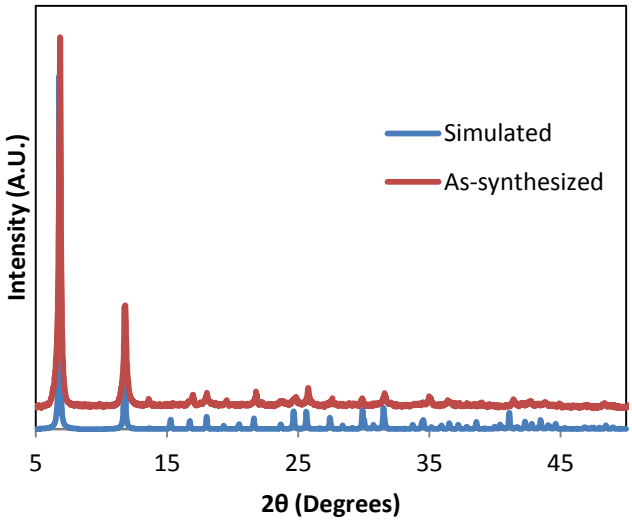

Figure A1. . PXRD of Mg-MOF-74 As-synthesized and Compared to Simulated

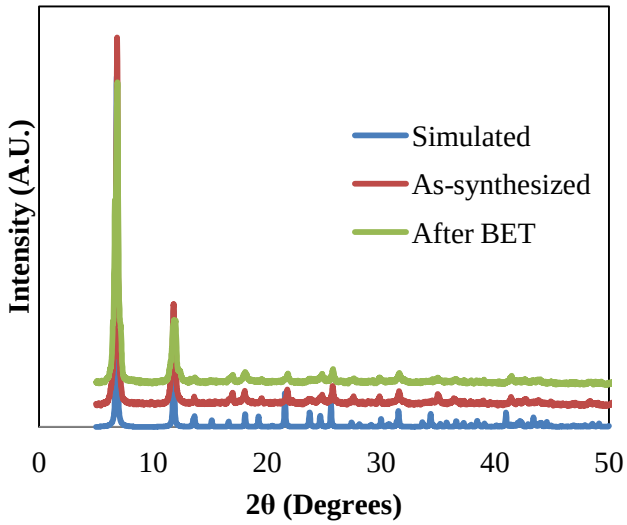

Figure A2. . PXRD of Zn-MOF-74 As-synthesized and after BET Compared to Simulated

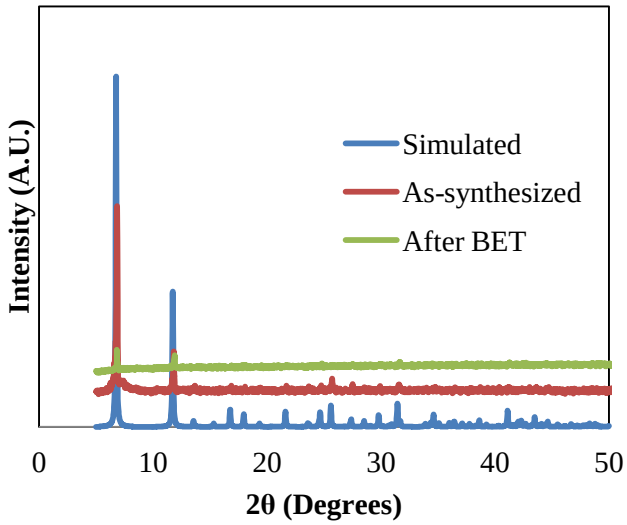

Figure A3. . PXRD of Co-MOF-74 As-synthesized and after BET Compared to Simulated

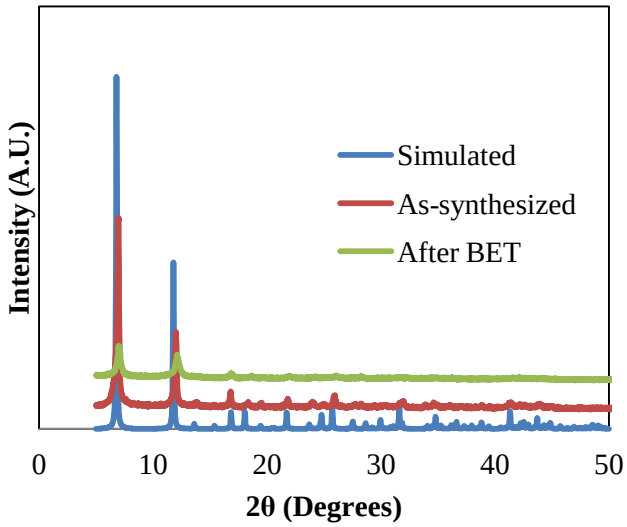

Figure A4. PXRD of Ni-MOF-74 As-synthesized and after BET Compared to Simulated

MOF-74 Materials used in CO Experiments

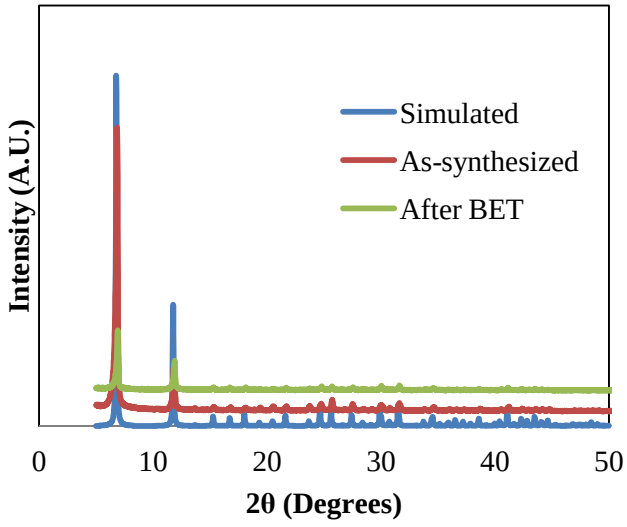

Figure A5. PXRD of Mg-MOF-74 As-synthesized and after BET Compared to Simulated (Different Batch)

Note that the PXRD of Zn-MOF-74 and Co-MOF-74 as-synthesized vs. simulated are the same as Figures A3 and A4 in the previous section since these same batches were used for both H_2O and CO experiments. Also note that the samples that N_2 adsorption was performed on to get BET surface areas were not subsequently used in experiments. Rather samples were taken from the original synthesis batch.

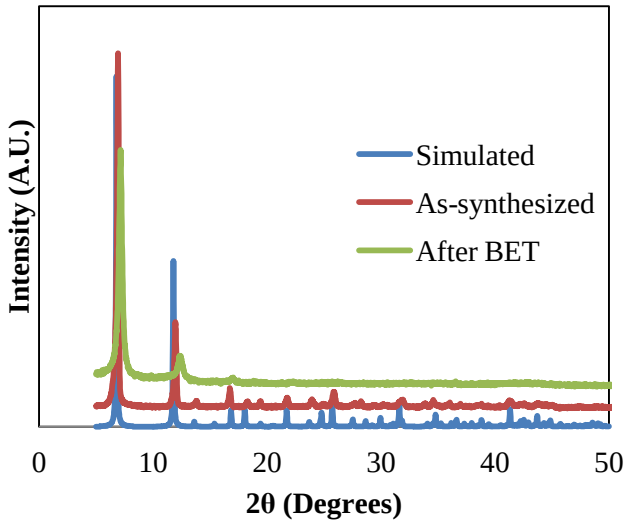

Figure A6. PXRD of Ni-MOF-74 As-synthesized and after BET Compared to Simulated (Different Batch)

APPENDIX B

TABLES OF H_2O ADSORPTION AND DESORPTION DATA

Table B1. H_2O Adsorption Desorption Data for Mg-MOF-74

%Relative Humidity	Weight (mg)	mmol of H_2O/g of MOF
Adsorption		
0.00	8.37	0.00
6.41	12.77	29.17
11.27	12.88	29.89
16.08	13.00	30.73
20.96	13.11	31.46
25.80	13.22	32.15
30.63	13.30	32.70
40.36	13.44	33.64
50.05	13.58	34.53
59.70	13.68	35.23
69.41	13.78	35.85
79.11	13.85	36.31
88.78	13.91	36.73
Desorption		
88.78	13.91	36.73
79.09	13.86	36.43
59.72	13.78	35.85
40.35	13.63	34.92
20.94	13.37	33.17
0.00	9.30	6.14

Table B2. H_2O Adsorption Desorption Data for Zn-MOF-74

%Relative Humidity	Weight (mg)	mmol of H_2O/g of MOF
Adsorption		
0.00	47.47	0.00
6.44	61.02	15.84
11.28	62.88	18.01
16.09	63.81	19.10
20.94	64.63	20.06
25.80	66.17	21.86
30.67	67.11	22.96
40.35	69.29	25.51
50.05	70.33	26.72
59.70	70.57	27.01
69.43	70.79	27.26
79.13	71.17	27.71
88.78	71.52	28.12
Desorption		
88.78	71.52	28.12
79.11	71.40	27.97
59.73	71.20	27.74
40.35	70.66	27.11
20.96	69.93	26.26
0.00	52.56	5.94

Table B3. H_2O Adsorption Desorption Data for Co-MOF-74

%Relative Humidity	Weight (mg)	mmol of H_2O/g of MOF
Adsorption		
0.00	111.05	0.00
10.65	159.52	24.23
20.50	161.54	25.24
30.33	162.94	25.94
40.18	164.16	26.55
50.03	164.84	26.89
59.87	165.32	27.13
69.70	165.86	27.39
79.55	166.09	27.51
89.38	166.39	27.66
Desorption		
89.38	166.39	27.66
79.54	166.25	27.59
59.87	165.71	27.32
40.19	164.86	26.90
20.50	162.75	25.84
0.00	120.00	4.47

Table B4. H_2O Adsorption Desorption Data for Ni-MOF-74

%Relative Humidity	Weight (mg)	mmol of H_2O/g of MOF
Adsorption		
0.00	32.60	0.00
10.65	42.72	17.23
20.51	43.31	18.23
30.34	43.69	18.88
40.18	44.12	19.61
50.02	44.81	20.78
59.86	44.89	20.91
69.72	45.14	21.35
79.54	46.19	23.13
89.38	46.29	23.30
Desorption		
89.38	46.29	23.30
79.54	46.25	23.23
59.87	46.06	22.91
40.19	45.71	22.32
20.50	45.21	21.47
0.00	36.18	6.10

APPENDIX C

RAW CO DATA COLLECTED ON THE PRESSURE DECAY SYSTEM

Table C1. Equilibrium Pressures (psia) Measured for Mg-MOF-74

Valve #3 before	Valve #4 before	Valve #3 after	Valve #4 after
298K			
5.67	0.00	2.74	1.95
10.4	1.95	5.73	5.12
15.1	5.12	9.58	8.95
20.1	8.95	13.7	13.5
40.3	13.5	25.1	24.5
65.2	24.5	42.0	41.6
95.1	41.6	64.5	64.4
97.7	64.4	78.9	78.5
313K			
5.10	0.00	2.43	1.87
10.5	1.87	6.44	4.74
15.3	4.74	9.32	8.96
20.3	8.96	13.8	13.6
40.2	13.6	24.9	24.8
65.3	24.8	42.1	41.9
95.3	41.9	65.0	64.6
99.7	64.6	79.9	79.4
333K			
5.61	0.00	2.61	2.10
10.1	2.10	5.70	5.32
15.1	5.32	9.63	9.27
20.1	9.27	14.0	13.8
40.2	13.8	25.1	24.9
65.2	24.9	42.2	42.0
95.5	42.0	65.0	64.9
100.3	64.9	80.4	79.8

Table C2. Equilibrium Pressures (psia) Measured for Zn-MOF-74

Valve #3 before	Valve #4 before	Valve #3 after	Valve #4 after
298K			
6.55	0.00	3.24	1.92
10.8	1.92	5.89	4.90
15.0	4.90	9.43	8.40
20.1	8.40	13.4	12.7
39.9	12.7	24.2	23.3
65.3	23.3	41.2	40.1
91.9	40.1	62.4	61.4
101.9	61.4	78.9	78.3
313K			
5.33	0.00	2.65	1.71
12.1	1.74	6.46	5.44
17.1	5.44	10.5	9.83
22.3	9.83	15.2	14.6
40.2	14.6	25.5	24.8
65.2	24.8	42.0	41.1
95.4	41.1	64.3	63.6
100.8	63.7	80.1	78.8
333K			
5.23	0.00	2.55	1.83
11.7	1.83	6.37	5.50
15.2	5.50	9.87	9.25
21.9	9.25	14.7	14.3
40.1	14.3	25.2	24.9
66.0	24.9	42.4	41.8
95.8	41.8	65.0	64.2
100.9	64.2	80.1	79.4

Table C3. Equilibrium Pressures (psia) Measured for Co-MOF-74

Valve #1 before	Valve #2 before	Valve #1 after	Valve #2 after
298K			
5.28	0.00	2.33	0.12
10.4	0.12	4.35	0.76
15.1	0.76	6.80	3.56
20.1	3.56	10.2	8.89
40.3	8.89	21.1	20.4
65.2	20.4	37.8	37.4
95.1	37.4	60.2	59.2
97.7	59.2	74.3	74.0
313K			
5.04	0.00	2.16	0.25
10.4	0.25	4.25	1.30
15.2	1.30	7.10	4.18
20.2	4.18	10.5	9.18
40.1	9.18	20.9	20.5
65.2	20.5	37.7	37.4
95.2	37.4	59.8	59.6
99.7	59.6	75.4	74.9
333K			
5.45	0.00	2.40	0.48
10.0	0.48	4.22	2.07
15.0	2.07	7.32	5.07
20.0	5.07	10.8	9.63
40.1	9.63	21.2	20.4
65.1	20.4	37.6	37.1
95.2	37.1	59.7	59.3
100.2	59.3	75.4	74.9

Table C4. Equilibrium Pressures (psia) Measured for Ni-MOF-74

Valve #3 before	Valve #4 before	Valve #3 after	Valve #4 after
298K			
4.91	0.00	2.41	0.14
13.1	0.14	5.80	3.45
17.1	3.45	9.48	8.93
25.2	8.93	16.0	15.7
44.9	15.7	28.4	28.2
69.2	28.2	45.9	45.8
96.1	45.8	67.8	67.2
100.1	67.2	81.5	81.4
313K			
6.23	0.00	2.84	0.38
10.3	0.39	4.81	2.87
15.6	2.87	8.55	7.67
42.5	7.67	24.0	21.3
65.3	21.3	40.4	40.0
95.1	40.0	64.2	63.4
100.0	63.4	79.5	79.0
94.0	79.0	85.6	85.3
333K			
5.58	0.00	2.67	0.63
11.7	0.63	5.66	3.15
15.1	3.42	8.70	7.65
20.1	7.65	13.1	12.6
40.2	12.6	24.5	24.2
70.2	24.2	44.1	43.8
91.7	43.8	64.7	64.3
102.4	64.3	80.8	80.7

Table C5. Properties of CO Needed for Peng Robinson Equation

T_c	132.7	K
P_c	507.34	psia
ω	0.049	
a	23079072.1	ml^2*psia/mol^2
b	24.539579	ml/mol
α	0.6017086	ml^2*psia/mol^2

APPENDIX D

TABLES AND GRAPHS OF EQUILIBRIUM PRESSURES AND LOADINGS CALCULATED FROM THE PENG ROBINSON EQUATION

Table D1. CO Adsorption Data for Mg-MOF-74

298 K		313 K		333 K	
Pressure (bar)	**mmol of CO/g**	**Pressure (bar)**	**mmol of CO/g**	**Pressure (bar)**	**mmol of CO/g**
0.000	0.000	0.000	0.000	0.000	0.000
0.134	0.132	0.129	0.074	0.145	0.076
0.353	0.309	0.326	0.172	0.366	0.139
0.617	0.476	0.617	0.305	0.639	0.219
0.929	0.627	0.940	0.427	0.951	0.267
1.689	0.894	1.709	0.656	1.719	0.430
2.871	1.178	2.889	0.910	2.898	0.627
4.440	1.447	4.451	1.153	4.473	0.809
5.410	1.576	5.474	1.276	5.500	0.935

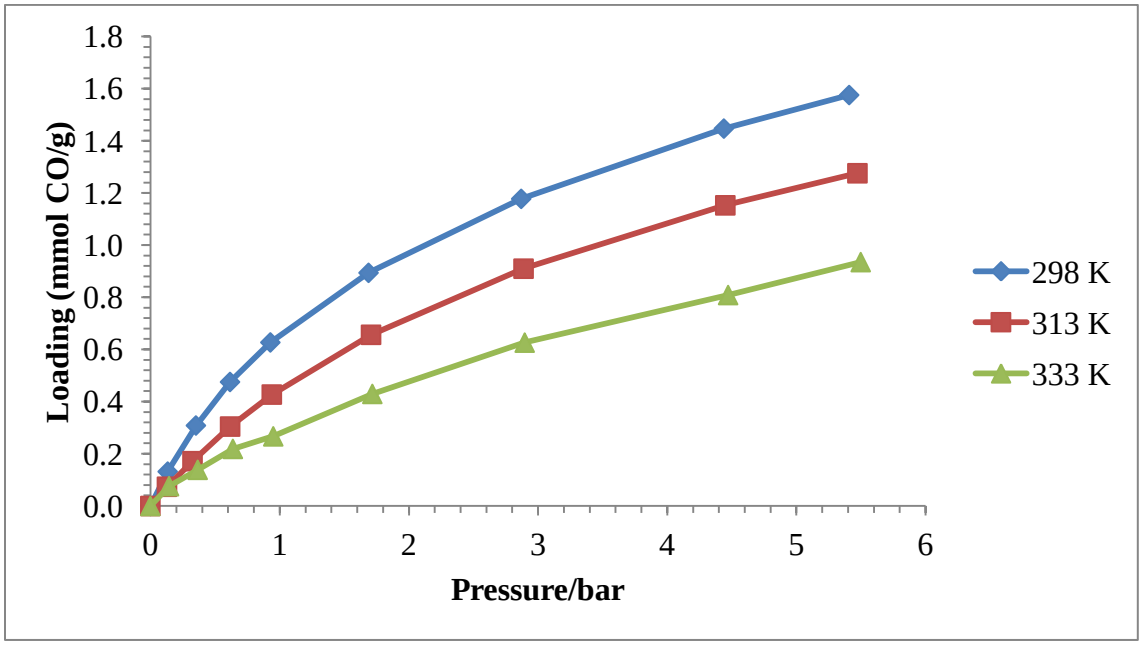

Figure D1. CO Data for Mg-MOF-74

Table D2. CO Adsorption Data for Zn-MOF-74

298 K		313 K		333 K	
Pressure (bar)	**mmol of CO/g**	**Pressure (bar)**	**mmol of CO/g**	**Pressure (bar)**	**mmol of CO/g**
0.000	0.000	0.000	0.000	0.000	0.000
0.132	0.250	0.118	0.133	0.126	0.083
0.338	0.565	0.375	0.376	0.379	0.225
0.579	0.883	0.677	0.636	0.637	0.345
0.877	1.209	1.010	0.889	0.986	0.515
1.604	1.805	1.707	1.329	1.714	0.820
2.766	2.457	2.836	1.882	2.885	1.229
4.232	2.999	4.387	2.428	4.429	1.670
5.395	3.306	5.432	2.723	5.478	1.911

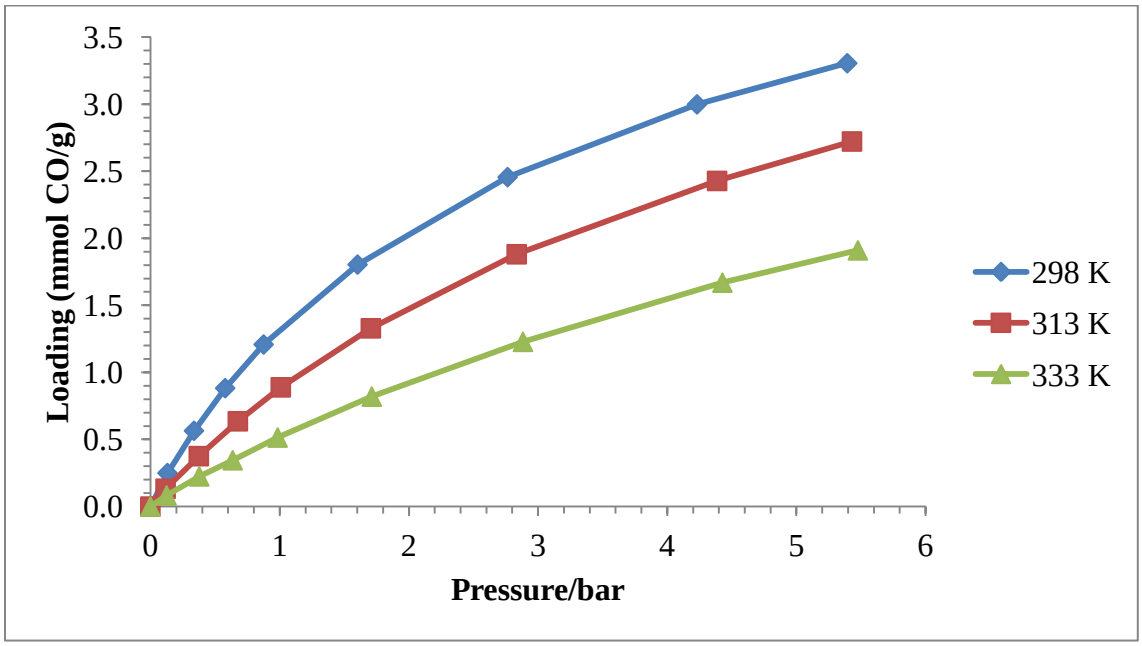

Figure D2. CO Data for Zn-MOF-74

Table D3. CO Adsorption Data for Co-MOF-74

298 K		313 K		333 K	
Pressure (bar)	**mmol of CO/g**	**Pressure (bar)**	**mmol of CO/g**	**Pressure (bar)**	**mmol of CO/g**
0.000	0.000	0.000	0.000	0.000	0.000
0.008	0.669	0.017	0.577	0.033	0.501
0.052	1.888	0.089	1.620	0.142	1.227
0.245	2.836	0.288	2.443	0.349	1.880
0.613	3.224	0.633	2.887	0.664	2.339
1.404	3.533	1.414	3.247	1.404	2.815
2.576	3.777	2.582	3.502	2.559	3.123
4.084	3.988	4.111	3.707	4.088	3.336
5.099	4.102	5.162	3.829	5.162	3.451

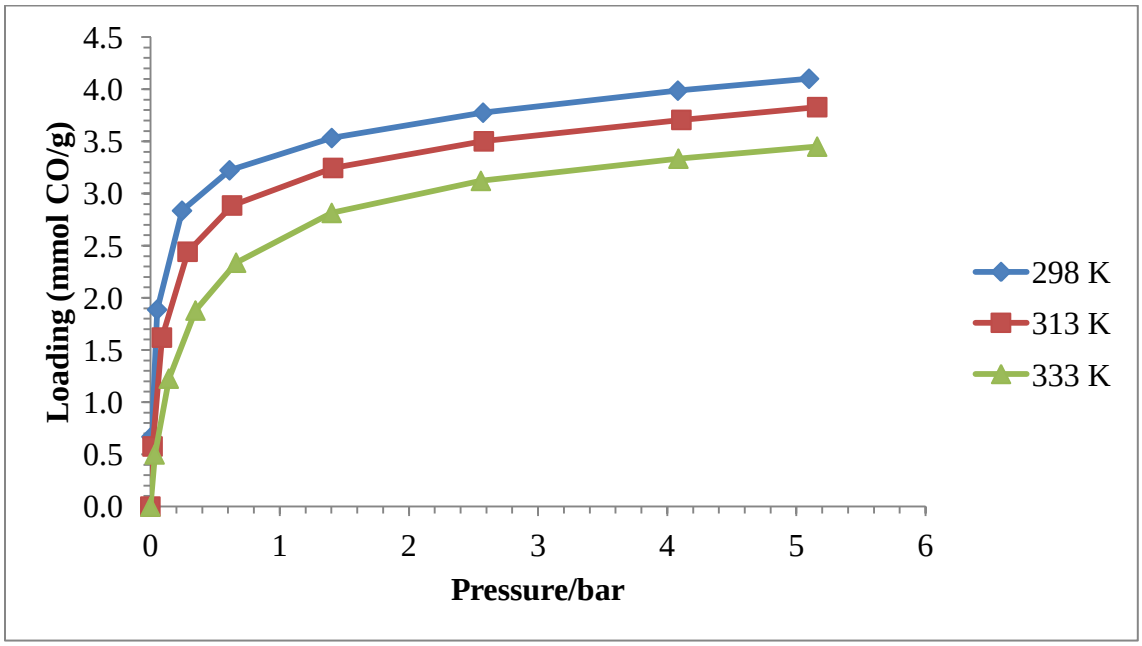

Figure D3. CO Data for Co-MOF-74

Table D4. CO Adsorption Data for Ni-MOF-74

298 K		313 K		333 K	
Pressure (bar)	**mmol of CO/g**	**Pressure (bar)**	**mmol of CO/g**	**Pressure (bar)**	**mmol of CO/g**
0.000	0.000	0.000	0.000	0.000	0.000
0.010	1.005	0.026	1.192	0.043	0.814
0.238	2.309	0.198	2.139	0.217	1.863
0.615	2.520	0.528	2.473	0.527	2.215
1.083	2.633	1.465	2.755	0.871	2.395
1.946	2.711	2.758	2.918	1.668	2.607
3.155	2.850	4.373	3.065	3.022	2.794
4.634	2.980	5.444	3.138	4.433	2.892
5.609	3.060	5.883	3.170	5.562	2.948

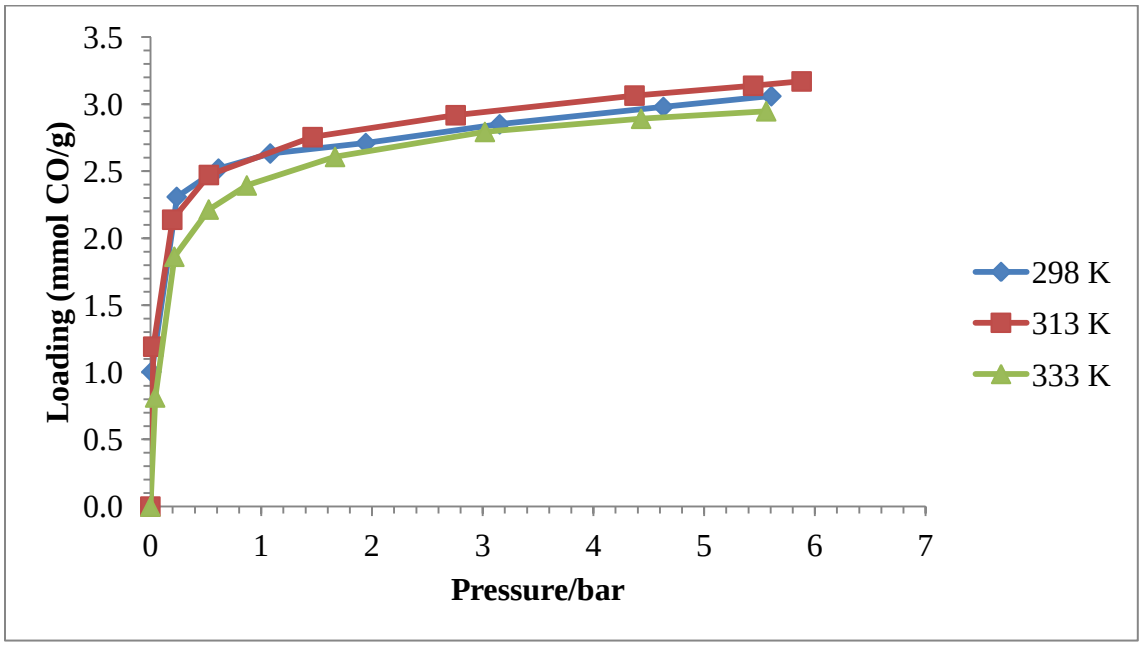

Figure D4. CO Data for Ni-MOF-74

This Figure is also shown in text as Figure 22.

APPENDIX E

TOTH EQUATION RESULTS

Table E1. Constants from Toth Equation Results

		Mg-MOF-74	Zn-MOF-74	Co-MOF-74	Ni-MOF-74
298 K	$C_{\mu s}$	3.770	6.063	4.539	3.429
	b	0.368	0.343	62.55	468.8
	t	0.585	0.790	0.484	0.373
313 K	$C_{\mu s}$	2.827	6.246	4.273	3.705
	b	0.224	0.182	18.02	193.1
	t	0.775	0.839	0.571	0.385
333 K	$C_{\mu s}$	3.748	7.366	4.110	3.154
	b	0.107	0.086	5.977	14.58
	t	0.627	0.753	0.623	0.662

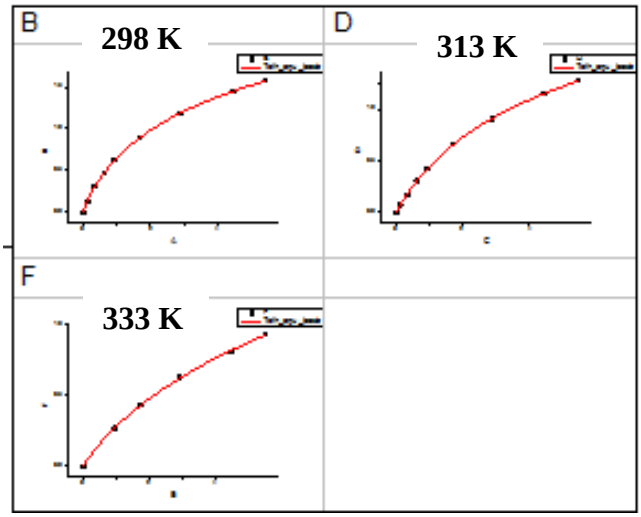

Figure E1. Print Screen of Toth equation Fit for Mg-MOF-74 (Without the 1st Three 333K Data Points) Created Using Origin Software

Table E2. Isosteric Heat of Adsorption Data for Mg-MOF-74

Loading	lnP at 298K	lnP at 313K	lnP at 333K	Slope = -Q/R	Q (kJ/mol)
0.1	-2.60	-1.81	-1.36	-3496.46	29.07
0.2	-1.88	-1.08	-0.64	-3495.33	29.06
0.3	-1.45	-0.63	-0.20	-3494.11	29.05
0.4	-1.13	-0.31	0.11	-3492.80	29.04
0.5	-0.88	-0.04	0.37	-3491.38	29.03
0.6	-0.66	0.19	0.58	-3489.86	29.01
0.7	-0.48	0.39	0.77	-3488.20	29.00
0.8	-0.31	0.57	0.93	-3486.39	28.99
0.9	-0.16	0.74	1.09	-3484.41	28.97

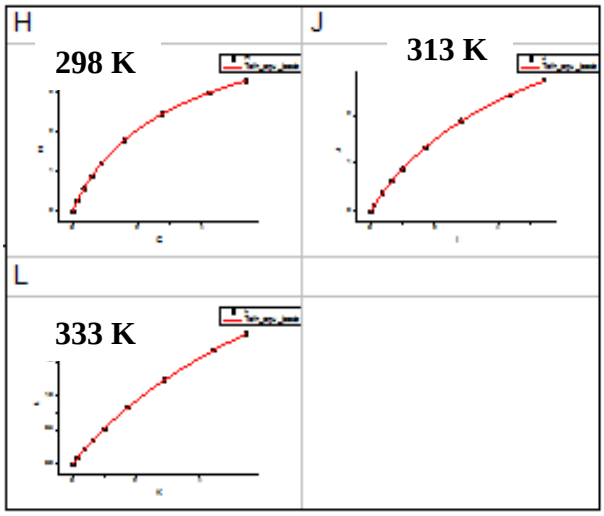

Figure E2. Print Screen of Toth Equation Fit for Zn-MOF-74 Created Using Origin Software

Table E3. Isosteric Heat of Adsorption Data for Zn-MOF-74

Loading	lnP at 298K	lnP at 313K	lnP at 333K	Slope = -Q/R	Q (kJ/mol)
0.1	-3.02	-2.42	-1.84	-3348.01	27.84
0.2	-2.31	-1.71	-1.13	-3339.20	27.76
0.3	-1.89	-1.28	-0.71	-3330.11	27.69
0.4	-1.58	-0.98	-0.41	-3320.73	27.61
0.5	-1.34	-0.74	-0.17	-3311.05	27.53
0.6	-1.14	-0.54	0.03	-3301.05	27.44
0.7	-0.97	-0.37	0.20	-3290.71	27.36
0.8	-0.81	-0.22	0.35	-3280.01	27.27
0.9	-0.68	-0.08	0.48	-3268.95	27.18
1	-0.55	0.04	0.60	-3257.49	27.08
1.1	-0.44	0.16	0.71	-3245.62	26.98
1.2	-0.33	0.27	0.81	-3233.31	26.88
1.3	-0.23	0.37	0.91	-3220.54	26.78
1.4	-0.13	0.46	1.00	-3207.29	26.67
1.5	-0.04	0.55	1.09	-3193.51	26.55
1.6	0.04	0.64	1.17	-3179.20	26.43
1.7	0.13	0.72	1.25	-3164.30	26.31
1.8	0.21	0.80	1.32	-3148.79	26.18
1.9	0.29	0.87	1.39	-3132.62	26.04

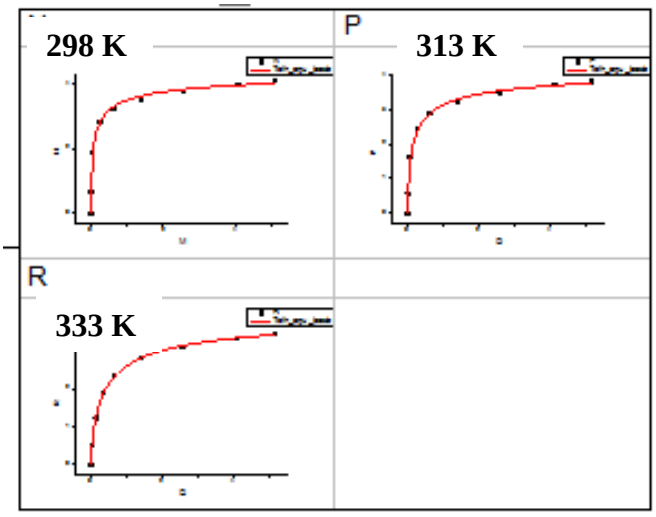

Figure E3. Print Screen of Toth Equation Fit for Co-MOF-74 Created Using Origin Software

Table E4. Isosteric Heat of Adsorption Data for Co-MOF-74

Loading	lnP at 298K	lnP at 313K	lnP at 333K	Slope = -Q/R	Q (kJ/mol)
0.1	-7.93	-6.62	-5.48	-6920.61	57.54
0.2	-7.21	-5.91	-4.76	-6927.56	57.60
0.3	-6.78	-5.48	-4.33	-6934.86	57.66
0.4	-6.47	-5.16	-4.02	-6942.52	57.72
0.5	-6.23	-4.91	-3.76	-6950.59	57.79
0.6	-6.02	-4.70	-3.55	-6959.10	57.86
0.7	-5.84	-4.52	-3.37	-6968.07	57.93
0.8	-5.68	-4.36	-3.21	-6977.56	58.01
0.9	-5.53	-4.21	-3.06	-6987.60	58.09
1	-5.40	-4.08	-2.92	-6998.25	58.18
1.1	-5.28	-3.95	-2.79	-7009.57	58.28
1.2	-5.16	-3.83	-2.67	-7021.61	58.38
1.3	-5.05	-3.72	-2.56	-7034.46	58.48
1.4	-4.94	-3.61	-2.45	-7048.19	58.60
1.5	-4.84	-3.51	-2.34	-7062.89	58.72
1.6	-4.74	-3.40	-2.24	-7078.69	58.85
1.7	-4.65	-3.31	-2.14	-7095.70	58.99
1.8	-4.56	-3.21	-2.04	-7114.06	59.15
1.9	-4.46	-3.11	-1.94	-7133.96	59.31
2	-4.37	-3.02	-1.84	-7155.58	59.49
2.1	-4.29	-2.93	-1.74	-7179.17	59.69
2.2	-4.20	-2.83	-1.65	-7205.00	59.90
2.3	-4.11	-2.74	-1.55	-7233.41	60.14
2.4	-4.02	-2.64	-1.45	-7264.82	60.40
2.5	-3.93	-2.55	-1.35	-7299.73	60.69
2.6	-3.84	-2.45	-1.24	-7338.75	61.01
2.7	-3.75	-2.35	-1.14	-7382.66	61.38
2.8	-3.66	-2.25	-1.03	-7432.46	61.79
2.9	-3.57	-2.14	-0.91	-7489.41	62.27
3	-3.47	-2.03	-0.79	-7555.20	62.81
3.1	-3.37	-1.92	-0.67	-7632.08	63.45
3.2	-3.26	-1.80	-0.53	-7723.15	64.21
3.3	-3.16	-1.67	-0.38	-7832.80	65.12
3.4	-3.04	-1.53	-0.22	-7967.47	66.24

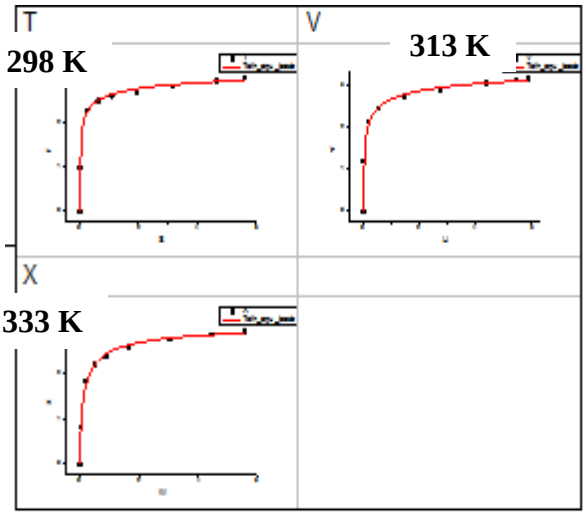

Figure E4. Print Screen of Toth Equation Fit for Ni-MOF-74 Created Using Origin Software

Table E5. Isosteric Heat of Adsorption Data for Ni-MOF-74

Loading	lnP at 298K	lnP at 313K	lnP at 333K	Slope = -Q/R	Q (kJ/mol)
0.1	-9.66	-8.85	-6.10	-10230.09	85.05
0.2	-8.93	-8.13	-5.37	-10238.64	85.12
0.3	-8.49	-7.69	-4.93	-10247.77	85.20
0.4	-8.17	-7.37	-4.61	-10257.52	85.28
0.5	-7.92	-7.12	-4.35	-10267.98	85.37
0.6	-7.70	-6.91	-4.13	-10279.21	85.46
0.7	-7.51	-6.72	-3.93	-10291.30	85.56
0.8	-7.34	-6.55	-3.76	-10304.36	85.67
0.9	-7.18	-6.40	-3.60	-10318.52	85.79
1	-7.04	-6.26	-3.45	-10333.90	85.92
1.1	-6.90	-6.13	-3.30	-10350.70	86.06
1.2	-6.77	-6.00	-3.17	-10369.09	86.21
1.3	-6.64	-5.88	-3.03	-10389.33	86.38
1.4	-6.52	-5.76	-2.90	-10411.71	86.56
1.5	-6.40	-5.65	-2.78	-10436.59	86.77
1.6	-6.28	-5.54	-2.65	-10464.41	87.00
1.7	-6.17	-5.43	-2.52	-10495.73	87.26
1.8	-6.05	-5.32	-2.39	-10531.26	87.56
1.9	-5.93	-5.21	-2.26	-10571.91	87.89
2	-5.81	-5.10	-2.13	-10618.88	88.29
2.1	-5.69	-4.99	-1.99	-10673.78	88.74
2.2	-5.57	-4.88	-1.84	-10738.81	89.28
2.3	-5.44	-4.77	-1.69	-10817.09	89.93
2.4	-5.30	-4.65	-1.52	-10913.17	90.73
2.5	-5.16	-4.53	-1.34	-11033.99	91.74
2.6	-5.01	-4.41	-1.13	-11190.70	93.04
2.7	-4.84	-4.28	-0.90	-11402.49	94.80
2.8	-4.66	-4.13	-0.61	-11705.72	97.32
2.9	-4.45	-3.98	-0.24	-12179.67	101.26

APPENDIX F

VIRIAL EQUATION RESULTS

Table F1. Constants from Virial Equation Results

		Mg-MOF-74	Zn-MOF-74	Co-MOF-74	Ni-MOF-74
298 K	B_0	0.099	0.722	4.297	46.18
	B_1	-0.761	-0.368	0.406	-92.50
	B_2	-0.057	0.041	-0.421	72.24
	B_3	-	-0.012	0.012	-24.08
	B_4	-	-	-	2.85
313 K	B_0	-0.520	0.161	3.699	22.80
	B_1	-0.594	-0.400	-0.242	-37.92
	B_2	-0.110	0.098	-0.090	27.50
	B_3	-	-0.024	-0.032	-8.77
	B_4	-	-	-	0.988
333 K	B_0	-1.063	-0.372	3.229	-1.21
	B_1	-0.757	-0.757	-1.195	10.16
	B_2	-0.015	0.464	0.385	-8.02
	B_3	-	-0.134	-0.100	2.46
	B_4	-	-	-	-0.299

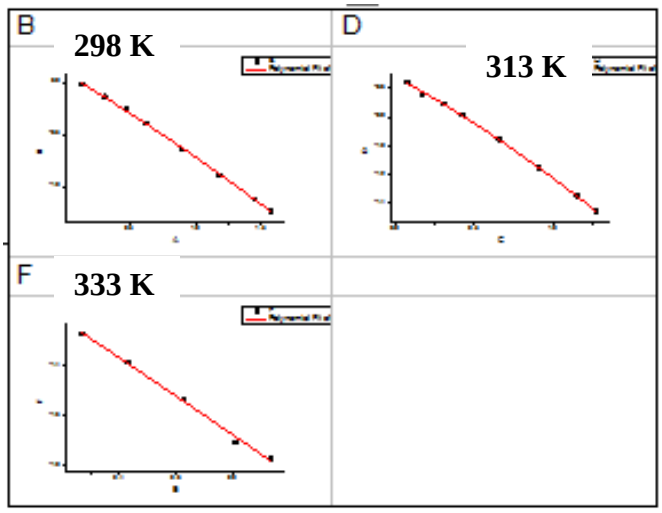

Figure F1. Print Screen of Virial Equation Fit for Mg-MOF-74 (Without the 1st Three 333K data Points) Created Using Origin Software

Table F2. Isosteric Heat of Adsorption Data for Mg-MOF-74

Loading	lnP at 298K	lnP at 313K	lnP at 333K	Slope = -Q/R	Q (kJ/mol)
0.1	-2.31	-1.72	-1.06	-3521.46	29.28
0.2	-1.55	-0.97	-0.36	-3369.21	28.01
0.3	-1.08	-0.50	0.09	-3287.88	27.34
0.4	-0.71	-0.14	0.44	-3257.68	27.08
0.5	-0.41	0.15	0.74	-3258.82	27.09
0.6	-0.14	0.41	1.01	-3271.52	27.20
0.7	0.10	0.63	1.25	-3275.99	27.24
0.8	0.32	0.84	1.47	-3252.44	27.04
0.9	0.53	1.04	1.65	-3181.09	26.45

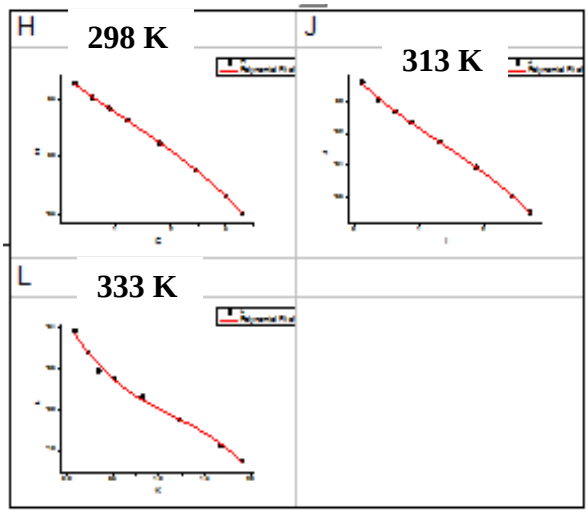

Figure F2. Print Screen of Virial Equation Fit for Zn-MOF-74 Created Using Origin Software

Table F3. Isosteric Heat of Adsorption Data for Zn-MOF-74

Loading	lnP at 298K	lnP at 313K	lnP at 333K	Slope = -Q/R	Q (kJ/mol)
0.1	-2.99	-2.42	-1.86	-3193.99	26.55
0.2	-2.26	-1.69	-1.10	-3272.60	27.21
0.3	-1.82	-1.25	-0.64	-3330.96	27.69
0.4	-1.50	-0.93	-0.31	-3371.18	28.03
0.5	-1.24	-0.68	-0.04	-3395.38	28.23
0.6	-1.02	-0.46	0.18	-3405.68	28.31
0.7	-0.84	-0.28	0.36	-3404.21	28.30
0.8	-0.67	-0.11	0.53	-3393.09	28.21
0.9	-0.52	0.03	0.67	-3374.43	28.05
1	-0.38	0.17	0.80	-3350.35	27.85
1.1	-0.25	0.29	0.92	-3322.97	27.63
1.2	-0.14	0.40	1.03	-3294.42	27.39
1.3	-0.02	0.51	1.13	-3266.81	27.16
1.4	0.08	0.61	1.23	-3242.26	26.96
1.5	0.19	0.71	1.32	-3222.90	26.80
1.6	0.28	0.80	1.41	-3210.84	26.69
1.7	0.38	0.89	1.51	-3208.21	26.67
1.8	0.47	0.97	1.60	-3217.12	26.75
1.9	0.56	1.06	1.70	-3239.69	26.93

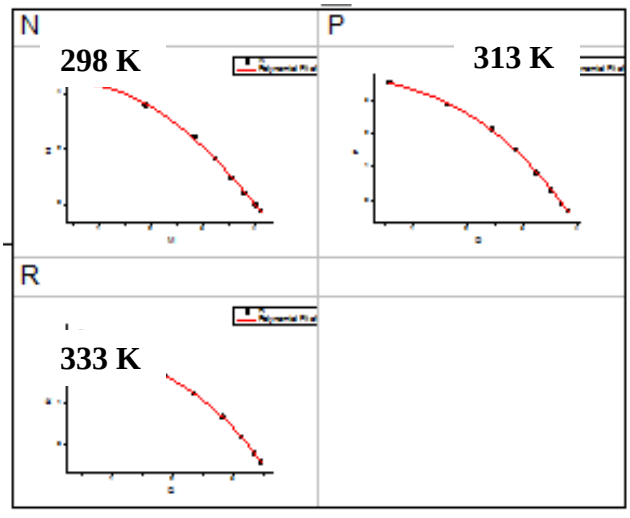

Figure F3. Print Screen of Virial Equation Fit for Co-MOF-74 Created Using Origin Software

Table F4. Isosteric Heat of Adsorption Data for Co-MOF-74

Loading	lnP at 298K	lnP at 313K	lnP at 333K	Slope = -Q/R	Q (kJ/mol)
0.1	-6.64	-5.98	-5.42	-3443.47	28.63
0.2	-5.97	-5.26	-4.61	-3832.56	31.86
0.3	-5.58	-4.82	-4.11	-4179.62	34.75
0.4	-5.31	-4.50	-3.72	-4486.55	37.30
0.5	-5.09	-4.24	-3.41	-4755.27	39.54
0.6	-4.90	-4.03	-3.14	-4987.69	41.47
0.7	-4.74	-3.83	-2.90	-5185.74	43.11
0.8	-4.58	-3.65	-2.69	-5351.31	44.49
0.9	-4.44	-3.49	-2.50	-5486.32	45.61
1	-4.29	-3.33	-2.32	-5592.69	46.50
1.1	-4.15	-3.19	-2.15	-5672.33	47.16
1.2	-4.02	-3.04	-1.99	-5727.15	47.62
1.3	-3.88	-2.90	-1.84	-5759.06	47.88
1.4	-3.74	-2.76	-1.70	-5769.99	47.97
1.5	-3.59	-2.62	-1.56	-5761.83	47.90
1.6	-3.45	-2.48	-1.42	-5736.51	47.69
1.7	-3.30	-2.34	-1.29	-5695.94	47.36
1.8	-3.15	-2.20	-1.15	-5642.02	46.91
1.9	-2.99	-2.05	-1.02	-5576.68	46.36
2	-2.83	-1.90	-0.89	-5501.83	45.74
2.1	-2.66	-1.75	-0.75	-5419.38	45.06
2.2	-2.49	-1.60	-0.61	-5331.24	44.32
2.3	-2.32	-1.44	-0.47	-5239.33	43.56
2.4	-2.14	-1.28	-0.32	-5145.55	42.78
2.5	-1.95	-1.11	-0.17	-5051.83	42.00
2.6	-1.76	-0.94	-0.01	-4960.07	41.24
2.7	-1.57	-0.76	0.15	-4872.19	40.51
2.8	-1.37	-0.58	0.32	-4790.11	39.82
2.9	-1.16	-0.39	0.50	-4715.72	39.21
3	-0.95	-0.19	0.69	-4650.96	38.67
3.1	-0.73	0.01	0.89	-4597.73	38.23
3.2	-0.51	0.22	1.09	-4557.94	37.89
3.3	-0.29	0.43	1.31	-4533.50	37.69
3.4	-0.06	0.66	1.54	-4526.34	37.63

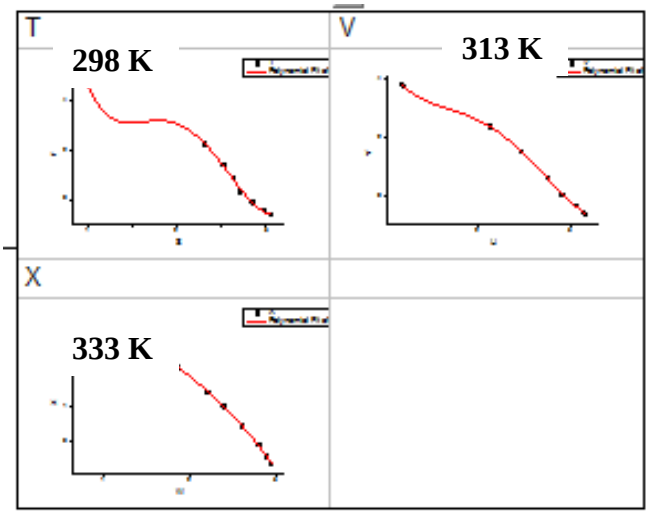

Figure F4. Print Screen of Virial Equation Fit for Ni-MOF-74 Created Using Origin Software

Table F5. Isosteric Heat of Adsorption Data for Ni-MOF-74

Loading	lnP at 298K	lnP at 313K	lnP at 333K	Slope = -Q/R	Q (kJ/mol)
0.1	-39.93	-21.58	-2.03	-107378.71	892.75
0.2	-31.99	-17.86	-2.13	-84656.93	703.84
0.3	-25.51	-14.87	-2.39	-65610.50	545.49
0.4	-20.19	-12.41	-2.64	-49843.93	414.40
0.5	-15.85	-10.37	-2.85	-36982.99	307.48
0.6	-12.37	-8.69	-3.00	-26674.72	221.77
0.7	-9.61	-7.32	-3.10	-18587.48	154.54
0.8	-7.47	-6.20	-3.14	-12410.89	103.18
0.9	-5.86	-5.31	-3.14	-7855.85	65.31
1	-4.69	-4.60	-3.08	-4654.56	38.70
1.1	-3.86	-4.05	-2.99	-2560.48	21.29
1.2	-3.32	-3.61	-2.87	-1348.38	11.21
1.3	-2.98	-3.28	-2.72	-814.29	6.77
1.4	-2.80	-3.01	-2.54	-775.52	6.45
1.5	-2.71	-2.80	-2.35	-1070.69	8.90
1.6	-2.68	-2.62	-2.14	-1559.68	12.97
1.7	-2.66	-2.46	-1.92	-2123.67	17.66
1.8	-2.62	-2.29	-1.68	-2665.09	22.16
1.9	-2.53	-2.12	-1.44	-3107.70	25.84
2	-2.38	-1.93	-1.19	-3396.50	28.24
2.1	-2.16	-1.71	-0.94	-3497.79	29.08
2.2	-1.86	-1.47	-0.67	-3399.17	28.26
2.3	-1.49	-1.19	-0.40	-3109.49	25.85
2.4	-1.05	-0.88	-0.12	-2658.91	22.11
2.5	-0.55	-0.55	0.17	-2098.86	17.45
2.6	-0.03	-0.19	0.47	-1502.05	12.49
2.7	0.48	0.18	0.80	-962.49	8.00
2.8	0.96	0.56	1.14	-595.44	4.95
2.9	1.36	0.93	1.52	-537.48	4.47

APPENDIX G

SAMPLE CALCULATIONS

Number of Molecules per Unit Cell for N_2 Adsorption onto Mg-MOF-74 used in H_2O Experiments

$$\frac{1400\ m^2}{g\ of\ MOF} \times \frac{3.63 \times 10^{-21}\ g\ of\ MOF}{unit\ cell} \times \frac{1\ molecule\ of\ N_2}{16.2\text{Å}^2} \times \frac{(1\text{Å}^2)}{(10^{-10})^2}$$

$$= 31.3\ \frac{N_2\ molecules}{unit\ cell}$$

Number of Molecules per Unit Cell for H_2O for Mg-MOF-74 (2nd point in Figure 11)

$$\frac{29.17\ mmol\ H_2O}{g\ of\ MOF} \times \frac{3.63 \times 10^{-21}\ g\ of\ MOF}{unit\ cell} \times \frac{6.022 \times 10^{23} molecules}{1\ mol\ of\ H_2O} \times \frac{1\ mol}{10^3 mmol}$$

$$= 63.71\ \frac{H_2O\ molecules}{unit\ cell}$$

Note that the calculations for the number of molecules per unit cell for CO are identical to those for H_2O.

Table G1. Calculation for Mass per Unit Cell (in absence of solvent molecules)

	C	H	O	Mg	Zn	Co	Ni
Asymmetric unit	4	1	3	1	1	1	1
Unit cell	72	18	54	18	18	18	18
Molar mass	12.01	1.008	16	24.31	65.39	58.93	58.69
Total (g/mol-unit cell)	864.72	18.144	864	437.58	1177.02	1060.74	1056.42
				2184.444	**2923.884**	**2807.604**	**2803.284**
Total (g/unit cell)				**3.63E-21**	**4.85534E-21**	**4.66E-21**	**4.66E-21**

REFERENCES

1. Morris, R.E. and P.S. Wheatley, *Gas storage in nanoporous materials.* Angewandte Chemie-International Edition, 2008. **47**(27): p. 4966-4981.

2. Caskey, S.R., A.G. Wong-Foy, and A.J. Matzger, *Dramatic tuning of carbon dioxide uptake via metal substitution in a coordination polymer with cylindrical pores.* Journal of the American Chemical Society, 2008. **130**(33): p. 10870-+.

3. Dietzel, P.D.C., R. Blom, and H. Fjellvag, *Base-induced formation of two magnesium metal-organic framework compounds with a bifunctional tetratopic ligand.* European Journal of Inorganic Chemistry, 2008(23): p. 3624-3632.

4. Dietzel, P.D.C., et al., *An in situ high-temperature single-crystal investigation of a dehydrated metal-organic framework compound and field-induced magnetization of one-dimensional metaloxygen chains.* Angewandte Chemie-International Edition, 2005. **44**(39): p. 6354-6358.

5. Rosi, N.L., et al., *Rod packings and metal-organic frameworks constructed from rod-shaped secondary building units.* Journal of the American Chemical Society, 2005. **127**(5): p. 1504-1518.

6. Glover, T.G., et al., *MOF-74 building unit has a direct impact on toxic gas adsorption.* Chemical Engineering Science, 2011. **66**(2): p. 163-170.

7. Dietzel, P.D.C., et al., *Hydrogen adsorption in a nickel based coordination polymer with open metal sites in the cylindrical cavities of the desolvated framework.* Chemical Communications, 2006(9): p. 959-961.

8. Schoenecker, P.M., et al., *Effect of Water Adsorption on Retention of Structure and Surface Area of Metal−Organic Frameworks.* Industrial & Engineering Chemistry Research, 2012.

9. Kizzie, A.C., A.G. Wong-Foy, and A.J. Matzger, *Effect of Humidity on the Performance of Microporous Coordination Polymers as Adsorbents for CO(2) Capture.* Langmuir, 2011. **27**(10): p. 6368-6373.

10. Xu, X.C., et al., *Separation of CO2 from power plant flue gas using a novel CO2 "molecular basket" adsorbent.* Abstracts of Papers of the American Chemical Society, 2003. **225**: p. U854-U855.

11. Liu, J., et al., *Stability Effects on CO(2) Adsorption for the DOBDC Series of Metal-Organic Frameworks.* Langmuir, 2011. **27**(18): p. 11451-11456.

12. Low, J.J., et al., *Virtual High Throughput Screening Confirmed Experimentally: Porous Coordination Polymer Hydration.* Journal of the American Chemical Society, 2009. **131**(43): p. 15834-15842.

13. Wang, Y. and M.D. Levan, *Adsorption Equilibrium of Carbon Dioxide and Water Vapor on Zeolites 5A and 13X and Silica Gel: Pure Components.* Journal of Chemical and Engineering Data, 2009. **54**(10): p. 2839-2844.

14. Andreini, C., et al., *Metal ions in biological catalysis: from enzyme databases to general principles.* Journal of Biological Inorganic Chemistry, 2008. **13**(8): p. 1205-1218.

15. Zhang, Y.G., *Electronegativities of Elements in Valence States and Their Applications. 2. A Scale for Strengths of Lewis Acids.* Inorganic Chemistry, 1982. **21**(11): p. 3889-3893.

16. Zhang, Y.G., *Electronegativities of Elements in Valence States and Their Applications .1. Electronegativities of Elements in Valence States.* Inorganic Chemistry, 1982. **21**(11): p. 3886-3889.

17. Britt, D., et al., *Highly efficient separation of carbon dioxide by a metal-organic framework replete with open metal sites.* Proceedings of the National Academy of Sciences of the United States of America, 2009. **106**(49): p. 20637-20640.

18. Millward, A.R. and O.M. Yaghi, *Metal-organic frameworks with exceptionally high capacity for storage of carbon dioxide at room temperature.* Journal of the American Chemical Society, 2005. **127**(51): p. 17998-17999.

19. Dietzel, P.D.C., et al., *Structural changes and coordinatively unsaturated metal atoms on dehydration of honeycomb analogous microporous metal-organic frameworks.* Chemistry-a European Journal, 2008. **14**(8): p. 2389-2397.

20. Bonino, F., et al., *Local structure of CPO-27-Ni metallorganic framework upon dehydration and coordination of NO.* Chemistry of Materials, 2008. **20**(15): p. 4957-4968.

21. Chavan, S., et al., *Response of CPO-27-Ni towards CO, N(2) and C(2)H(4).* Physical Chemistry Chemical Physics, 2009. **11**(42): p. 9811-9822.

22. Rouquerol, F., J. Rouquerol, and K. Sing, *Adsorption by Powders and Porous Solids- Principles, Methodoloy and Applications*. 1999: Academic Press.

23. Chavan, S., et al., *CO Adsorption on CPO-27-Ni Coordination Polymer: Spectroscopic Features and Interaction Energy.* Journal of Physical Chemistry C, 2009. **113**(8): p. 3292-3299.

24. Xie, Y.C., et al., *Zeolites modified by CuCl for separating CO from gas mixtures containing CO2.* Adsorption-Journal of the International Adsorption Society, 1996. **3**(1): p. 27-32.

25. Rayner-Canham, G. and T. Overton, *Descriptive Inorganic Chemistry*. 2003: W. H. Freeman and Company.

26. Theophanides, T., *FTIR Spectroscopy of Adsorbed Probe Molecules for Analyzing the Surface Properties of Supported Pt (Pd) Catalysts*, in *Infrared Spectroscopy - Materials Science, Engineering and Technology*, T. Theophanides, Editor. 2012, InTech. p. 510.

27. Valenzano, L., et al., *Computational and Experimental Studies on the Adsorption of CO, N(2), and CO(2) on Mg-MOF-74.* Journal of Physical Chemistry C, 2010. **114**(25): p. 11185-11191.

28. Saha, D. and S. Deng, *Adsorption Equilibria and Kinetics of Carbon Monoxide on Zeolite 5A, 13X, MOF-5, and MOF-177.* Journal of Chemical and Engineering Data, 2009. **54**(8): p. 2245-2250.

29. Karra, J.R. and K.S. Walton, *Effect of open metal sites on adsorption of polar and nonpolar molecules in metal-organic framework Cu-BTC.* Langmuir, 2008. **24**(16): p. 8620-8626.

30. Karra, J.R. and K.S. Walton, *Molecular Simulations and Experimental Studies of CO(2), CO, and N(2) Adsorption in Metal-Organic Frameworks.* Journal of Physical Chemistry C, 2010. **114**(37): p. 15735-15740.

31. Neyman, K.M. and N. Rosch, *Bonding and vibrations of CO molecules adsorbed at transition metal impurity sites on the MgO(001) surface. A density-functional model cluster study.* Chemical Physics, 1993. **177**(2): p. 561-570.

32. Scarano, D., et al., *CO Adsorption at 77-K ON CoO/MgO and NiO/MgO Solid-Solutions: A Fourier-transform Infrared Study.* Journal of the Chemical Society-Faraday Transactions, 1992. **88**(3): p. 291-296.

33. Do, D.D., *Adsorption Analysis: Equilibria and Kinetics*, ed. R.T. Yang. 1998, London: Imperial College Press.

34. Valenzano, L., et al., *Heats of Adsorption of CO and CO(2) in Metal-Organic Frameworks: Quantum Mechanical Study of CPO-27-M (M = Mg, Ni, Zn).* Journal of Physical Chemistry C, 2011. **115**(44): p. 21777-21784.

35. Toreki, R. *Rob Toreki's Organomettalic HyperTextBook*. 2003 11/20/2003 [cited 2012 05/19/2012]; Available from: http://www.ilpi.com/organomet/carbonyl.html.

36. Evans, M. *The Organometallic Reader Epic Ligand Survey: Carbon Monoxide*. 2012 01/17/2012 [cited 2012 05/20/2012]; Available from: http://organometallicchem.wordpress.com/2012/01/17/epic-ligand-survey-carbon-monoxide/.

37. Triebe, R.W. and F.H. Tezel, *Adsorption of Nitrogen, Carbon-Monoxide, Carbon-Dioxide and Nitric-Oxide on Molecular-Sieves.* Gas Separation & Purification, 1995. **9**(4): p. 223-230.

38. Lopes, F.V.S., et al., *Adsorption of H2, CO2, CH4, CO, N2 and H2O in Activated Carbon and Zeolite for Hydrogen Production.* Separation Science and Technology, 2009. **44**(5): p. 1045-1073.

39. Grande, C.A., et al., *Adsorption of off-gases from steam methane reforming (H-2, CO2, CH4, CO and N-2) on activated carbon.* Separation Science and Technology, 2008. **43**(6): p. 1338-1364.

40. Wang, Q.M., et al., *Metallo-organic molecular sieve for gas separation and purification.* Microporous and Mesoporous Materials, 2002. **55**(2): p. 217-230.

41. Chowdhury, P., et al., *Adsorption of CO, CO2 and CH4 on Cu-BTC and MIL-101 metal organic frameworks: Effect of open metal sites and adsorbate polarity.* Microporous and Mesoporous Materials, 2012. **152**: p. 246-252.

42. Song, L., et al., *Investigation of adsorption hysteresis in microporous materials*, in *Recent Advances in the Science and Technology of Zeolites and Related Materials, Pts a - C*, E. VanSteen, M. Claeys, and L.H. Callanan, Editors. 2004. p. 1797-1803.

43. Zhou, W., H. Wu, and T. Yildirim, *Enhanced H(2) Adsorption in Isostructural Metal-Organic Frameworks with Open Metal Sites: Strong Dependence of the Binding Strength on Metal Ions.* Journal of the American Chemical Society, 2008. **130**(46): p. 15268-+.

44. Dietzel, P.C., R. Blom, and H. Fjellvag, *Coordination Polymers Based on the 2,5-Dihydroxyterephthalate Ion and Alkaline Earth Metal (Ca, Sr) and Manganese Cations.* Zeitschrift Fur Anorganische Und Allgemeine Chemie, 2009. **635**(12): p. 1953-1958.

45. Chemistry Department, W.P.I. *Lewis Acids and Bases-Hard and Soft Acid/Base Theory*. 2004 1/13/2004 [cited 2012 05/24/2012].